General Disclaimer

One or more of the Following Statements may affect this Document

- This document has been reproduced from the best copy furnished by the organizational source. It is being released in the interest of making available as much information as possible.

- This document may contain data, which exceeds the sheet parameters. It was furnished in this condition by the organizational source and is the best copy available.

- This document may contain tone-on-tone or color graphs, charts and/or pictures, which have been reproduced in black and white.

- This document is paginated as submitted by the original source.

- Portions of this document are not fully legible due to the historical nature of some of the material. However, it is the best reproduction available from the original submission.

NASA
National Aeronautics and Space Administration

NASA CR-135260
SwRI 02-4492

STUDY OF LIQUID JET IMPINGEMENT ON SCREENS

by

Franklin T. Dodge
Randall E. Ricker

SOUTHWEST RESEARCH INSTITUTE
San Antonio, Texas

prepared for

NATIONAL AERONAUTICS AND SPACE ADMINISTRATION

NASA Lewis Research Center
Contract NAS 3-20086

1. Report No.	2. Government Accession No.	3. Recipient's Catalog No.
NASA CR-135260		

4. Title and Subtitle	5. Report Date
Study of Liquid Jet Impingement on Screens	Sept. 1976
	6. Performing Organization Code

7. Author(s)	8. Performing Organization Report No.
Franklin T. Dodge Randall E. Ricker	Final Report, 02-4492
	10. Work Unit No.
9. Performing Organization Name and Address Southwest Research Institute 6220 Culebra Rd San Antonio, Texas 78284	11. Contract or Grant No. NAS3-20086
	13. Type of Report and Period Covered Contractor Report
12. Sponsoring Agency Name and Address National Aeronautics and Space Administration Washington, D.C. 20546	14. Sponsoring Agency Code

15. Supplementary Notes

Project Manager, E. P. Symons, Propulsion and Power Division,
NASA Lewis Research Center, Cleveland, Ohio 44135

16. Abstract

Previously developed analytical models relate pressure drop across a fine-mesh screen to through-flow velocity for duct systems. These models are shown to be unreliable for an unconfined flow, such as a free jet, impinging on a screen. A new model is developed for these kinds of systems, incorporating the important influence of liquid deflection by the screen. A new parameter, the boundary layer blockage coefficient, is introduced. This coefficient depends on the screen weave geometry and the jet impingement angle, and essentially accounts for the increase in fluid particle trajectory length through the screen resulting from the flow deflection. Comparisons are made with previous experimental studies to determine empirical values of the blockage coefficient. It is concluded that the new model reliably predicts the bulk flow and penetration characteristics of an impinging liquid jet interacting with a screen.

17. Key Words (Suggested by Author(s))	18. Distribution Statement
Low-gravity, Jet Impingement, Propellant Control, Screen Acquisition Systems, Fluid Mechanics	Unclassified - unlimited

19. Security Classif. (of this report)	20. Security Classif. (of this page)	21. No. of Pages	22. Price*
Unclassified	Unclassified	47 + prelims + dist. list	

* For sale by the National Technical Information Service, Springfield, Virginia 22151

INTRODUCTION

Many types of engineering equipment require the flow of fluids through screens. Typical applications include filters, thickeners, paper-making machines, and coalescers. Recent studies have shown that fine-mesh screens also make an excellent system for controlling liquids in spacecraft propellant tanks during periods of reduced gravity. Surface tension forces between the screen wires and the liquid selectively exclude vapor, thereby containing liquid at a desired location. Typical applications for these devices are the providing of vapor-free liquid for restarting an engine and for liquid transfer from one storage tank to another. To be successful, the devices must be capable of being refilled after use. To date, considerable effort has been expended in studying basic characteristics such as wicking and flow-through pressure drop, but relatively little effort has been spent on fundamental understanding of liquid behavior during refilling.

Several investigators have developed correlations relating the velocity V through a screen and the pressure drop ΔP across the screen. Most correlations can be put in a form equivalent to the one developed by Armour and Cannon (ref. 1):

$$\Delta P = \alpha\left(\frac{a^2 bQ}{\varepsilon^2}\right)\mu V + \beta\left(\frac{bQ}{\varepsilon^2 D}\right)\rho V^2 \qquad (1)$$

One exception to this statement is the model developed in reference 5, for square-mesh screens, which relates ΔP and V linearly. The geometry of the screen weave is represented by: ε, the void volume ratio; a, the ratio of unit surface area to unit volume; b, the screen thickness; D, the pore diameter or particle-retention rating; and Q, a tortuosity factor, the ratio of a typical fluid path length to the screen thickness. Fluid properties are represented by viscosity μ and density ρ. Both α and β are empirical factors which represent, respectively, viscous and inertial contributions to ΔP. Armour and Cannon's tests gave

universal factors for α of 8.61 and β of 0.52. More recent tests (refs. 2 and 3, for example) indicate that these parameters depend upon the screen weave.

All correlations of the form of equation (1) have been developed for uniform, unidirectional flow confined by the walls of a tube, across a perpendicularly-oriented screen. For space applications, it is unlikely that the refilling liquid will be confined; some sort of free-jet or free-flow process is more reasonable. Tests of the impingement of a circular jet of liquid upon various screens under weightless conditions (ref. 4) have shown in fact that equation (1) overpredicts the through-flow by a considerable margin, a conclusion arrived at by interpreting ΔP as the average pressure (i.e., the impact force of the jet divided by the impact area) on the upstream screen surface. Much of the liquid was simply deflected as if by a baffle.

The analysis presented in this report was undertaken to help gain an understanding of the impingement of a liquid jet on a screen. Specific objectives were:

- Develop a mathematical model for predicting the through-flow of a circular jet of liquid impinging normally or at an angle (45°) onto the surface of a fine-mesh screen.
- Compare and rationalize the model with existing NASA data.
- Define additional experiments to provide an increased degree of confidence in the model.

Computer or wholly numerical models have been excluded, to emphasize physical understanding and to enable the model to be used economically for design and parametric studies.

MODELING OF SCREEN THROUGH-FLOW

Modeling Approach

Analysis of flow through a screen requires knowledge of the driving pressure distribution at all points on the screen. Thus, the first modeling task is to derive expressions for the pressures; potential flow theory is used for this. Next, a physical model of the flow within and through the screen is proposed, using equation (1) as a starting point; the formulation of this flow model constitutes the main original effort of the analysis.

Impingement Pressures

Ideal, irrotational, incompressible flow is used to compute the pressures exerted on the screen by the impinging circular jet, and the screen is idealized as a rigid impermeable plane. Most liquids used for space applications have small viscosities, so viscous effects are important only in the boundary layer. (Boundary layer effects are incorporated in the screen through-flow model.) Since the emerging jet has a velocity which is only a small fraction of the impingement velocity (ref. 4), its momentum is negligible in the first approximation, and thus the assumption of an impermeable screen is reasonable for computing impact pressures.

A previous theory (ref. 6) predicts both pressure and tangential velocity distributions for normal impingement of a circular jet on an impermeable plane. To obtain predictions that are more directly usable, however, an independent numerical computation was made (Appendix A). These results show that the pressure and tangential (radial) velocity distributions can be closely approximated by the simple expressions:

$$\Delta P = \frac{1}{2} \rho C_p V_j^2 \tag{2}$$

$$C_p = 1 - 0.221(r/R_j)^{2.28} \tag{3}$$

$$V_r = 0.515V_j(r/R_j) \tag{4}$$

In developing the through-flow model, it is more convenient to approximate these relations by ones that can be analytically integrated in certain expressions. The additional approximations are:

$$C_p = 1 - 0.25(r/R_j)^2 \tag{5}$$

$$V_r = 0.5V_j(r/R_j) \tag{6}$$

There is only a small difference between equations (3) and (5), or between (4) and (6). Furthermore, the impact force, $\pi\rho V_j^2 R_j^2$, and the relation between C_p and V_j, namely $C_p = 1 - (V_r/V_j)^2$, are given exactly by both approximations. Incidentally, positive ΔP implies that liquid will flow through the screen. Thus, equation (5) indirectly verifies the conclusion of reference 4 that the emerging jet has a diameter about twice that of the impinging jet, since $C_p \geq 0$ for $r \leq 2R_j$.

Previously developed models for oblique impingement apply only to two-dimensional or rectangular jets (refs. 6 and 7). Numerical solutions, even for one angle of obliquity, are impractical. Consequently, an approximate procedure described in Appendix A is used to predict the pressure distribution. To get integrable expressions for C_p, analytical expressions are required; these approximations are:

$$C_p = 1 - 0.25(r/R_j)^2 \qquad -90° \leq \theta \leq 90° \tag{7}$$

$$C_p = [1 - (r/R_j)^2]\cos^2\theta + [1 - 0.25(r/R_j)^2]\sin^2\theta \qquad 90° \leq \theta \leq 270° \tag{8}$$

$$V_r = 0.5V_j\left[r\Big/\left(1 + \frac{1}{2}\cos\theta\right)R_j\right] \tag{9}$$

The coordinate system is shown in the sketch. Equation (7) neglects a region of small pressures shown schematically by the shaded area (see also discussion in Appendix A and Figure A-3). Also, for the term multiplied by $\cos^2\theta$ in equation (8), r must be limited to values less than R_j. The total force, $\pi\rho V^2 R^2 \cos\theta$, is overpredicted by equations (7) and (8), but by less than fifteen percent.

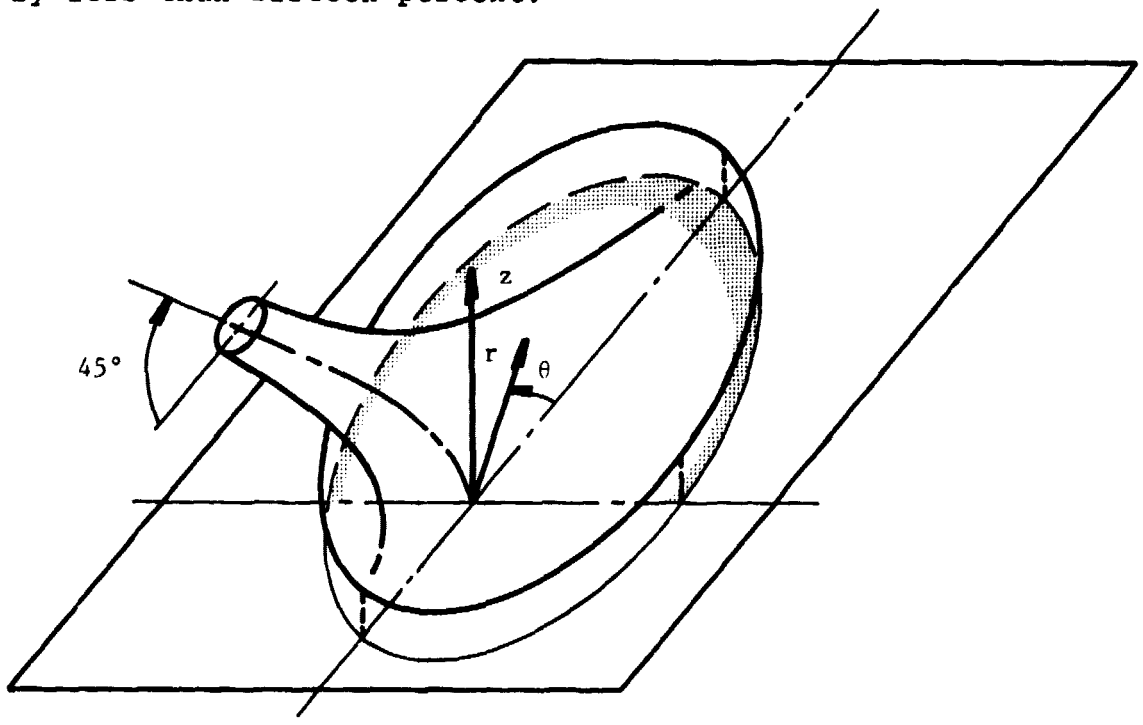

Predictions of Unmodified Model

The applicability of the duct-flow relation between pressure and velocity, equation (1), can be determined by substituting equation (5), for normal impingement, or equations (7) and (8), for 45° oblique impingement into equation (1). The solution for V is

$$V = \frac{A\mu}{2B\rho}\left[\sqrt{1 + \frac{2C_p V_j^2}{B}\left(\frac{\rho B}{\mu A}\right)^2} - 1\right] \qquad (10)$$

where $A = \alpha(a^2 bQ/\varepsilon^2)$ and $B = \beta(bQ/D\varepsilon^2)$. Equation (10) gives the velocity of the emergent jet as a function of r since C_p depends

on r. To compare this equation with test results, it is necessary to make the assumption that the <u>average</u> velocity over the area of the emergent jet corresponds to the <u>measured</u> velocity with which the jet leaves the screen as a growing geyser (ref. 4).

The average velocity for normal impingement is derived by integration over the range of r for which $\Delta P \geq 0$, namely $0 \leq r \leq 2R_j$. The result is

$$V_{av} = \frac{\mu A}{6\rho}\left(\frac{\mu A}{\rho B V_j}\right)^2 \left\{ \left[1 + \frac{2}{B}\left(\frac{\rho B V_j}{\mu A}\right)^2 \right]^{3/2} - 1 \right\} - \frac{\mu A}{2\rho B} \qquad (11)$$

This expression overpredicts the test data of ref. 4 by about 100 percent, on average. Reference 4 proposed an empirical correlation for V_{av} which essentially amounts to the use of an average C_p of 1/8, rather than the 1/4 resulting from equation (5); that is, the effective pressure is supposed to be one-half the actual average pressure. Predictions from this correlation are within ±15 percent of the test data (ref. 4). There is no apparent underlying reason that can explain a reduction of ΔP by a factor of 2; consequently, the correlation may not be reliable for other test data. In any case it does not aid in understanding screen-flow mechanics and so cannot be extended to other kinds of potential applications involving unconfined flows unless first verified by experimental data.

The duct-flow model also overestimates test data for 45° impingement by about 100 percent.

Impinging Jet Screen-Flow Model

Since the duct-flow screen model does not give reliable predictions of the through-flow for jet impingement, a new or modified model is required. It seems likely that liquid flowing along the plane of the screen or tangentially within the screen is the reason for the failure of the duct-flow model. The duct-flow model assumes a more or less straight-through path for the liquid, but liquid will be deflected into the plane of the screen

for all unconfined flows. There is an additional pressure drop caused by the increase in the flow-path length resulting from the flow deflection which is not included in the duct-flow model. This additional ΔP can be incorporated into a screen-flow model in several ways. The original basis of equation (1), namely that the pressure drop is caused by a combination of viscous flow around the screen wires and inertial losses through parallel interconnecting channels between the wires, could be altered by assuming the screen to be a porous medium. Or the basic assumptions of equation (1) could be kept, but the trajectory of the flow altered to account for the in-plane component.

For closely woven screens such as the twilled Dutch weave shown in the sketch, it may be plausible to idealize a screen as a sort of porous medium. It is further plausible that the

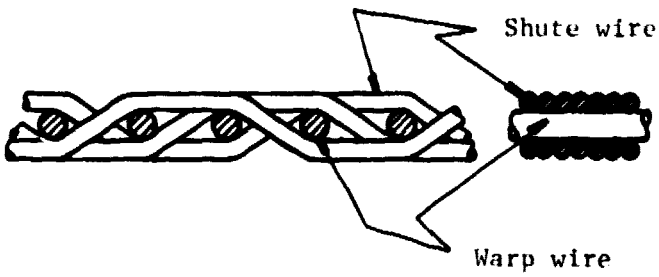

internal resistance for tangential flow in the plane of the screen is less than the resistance for flow across the thickness; in fact, according to the theory developed in Appendix C, this is required in order to make the predicted through-flows agree with the test data of reference 4. Simple calculations (Appendix C) show that the in-plane resistance must be less than 1/1000 of the through-flow resistance to obtain correlation between test and theory. A flow resistance ratio of 1/1000 corresponds, roughly, to average pore diameters in the plane of the screen that are at least 30 times larger (for inertial losses) or 1000 times larger (for viscous losses) than the pores in the through-flow direction. These values seem too large to be reasonable. Thus, the porous medium model is probably not physically realistic.

Models which retain the basic assumptions of equation (1) can account for the non-direct flow path by increasing the tortuosity factor, Q, as shown conceptually by the sketches. The

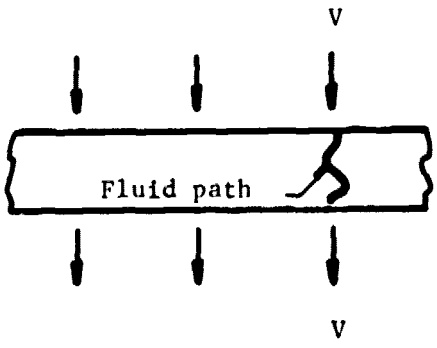

Duct Flow, $Q \simeq 1.3$

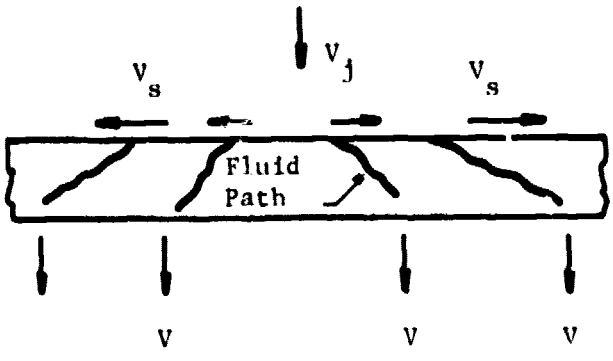

Jet Impingement Flow, $Q > 1.3$

modified tortuosity factor can be estimated by assuming that the flow paths are inclined at an angle which is determined by both the through-flow velocity V and the tangential velocity V_s. The flow path length is then $\ell = bQ(V^2 + V_s^2)^{1/2}/V$. Note that the length varies over the impingement since both V and V_s are functions of r. For this model, equation (1) is modified to account for jet impingement dynamics by replacing the flow length bQ by ℓ, and V by $(V^2 + V_s^2)^{1/2}$. Thus, the expression

$$\Delta P = \alpha\left(\frac{a^2 bQ}{\varepsilon^2}\right)\mu\left(\frac{V^2 + V_s^2}{V}\right) + \beta\left(\frac{bQ}{\varepsilon^2 D}\right)\rho\left[\frac{(V^2 + V_s^2)^{3/2}}{V}\right] \qquad (12)$$

is the pressure-velocity relation for this model. Although this model predicts a reduction in V for a given ΔP when compared to equation (1), it has several shortcomings. First, the flow paths cannot be inclined at all angles throughout the range 0° to 90°. Equation (12) requires this, however, since: $V_s = 0$ and $V > 0$ near the stagnation point of the jet, which gives an inclination of 0°; and $V = 0$ and $V_s > 0$ near the emerging jet periphery, which gives an inclination of 90°. Second, for large inclination angles, the viscous shear forces at the interface

between the screen and the impinging jet have significant components in the flow-path direction; this, as well as ΔP, helps drive the flow. Equation (12) neglects the shear force. It is evident that by doing so an unrealistically large ΔP is required near the periphery where the through-flow is small ($V \approx 0$), since V_s is large there. The contribution to the total through-flow of the peripheral parts of the jet is small, however, and equation (12) may model the important central parts of the through-flow fairly accurately. The overall effect of V_s in this model is unrealistic, nonetheless, because of the unbounded behavior of the terms V_s^3/V and V_s^2/V as $V \to 0$.

To correct these deficiencies, a further modification is proposed. As shown in the sketch (for a twilled Dutch weave) the shute wires which extend into the boundary layer intercept a part of the tangential velocity. The intercepted tangential velocity is ϕV_s, where ϕ is a "blockage" coefficient which may

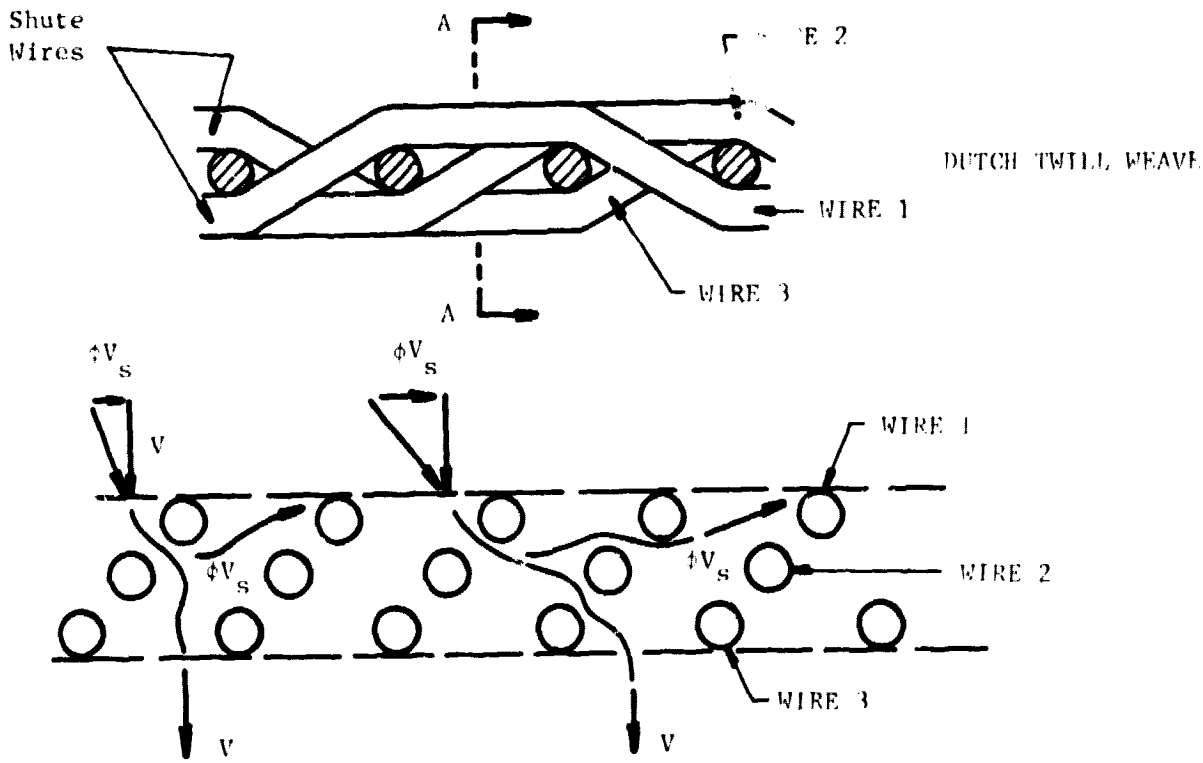

depend on both the screen and the jet geometries. As before the tangential velocity ϕV_s, combined with V, effectively selects a

flow path inclined at the angle arctan $(V/\phi V_s)$. The coefficient ϕ accounts for a number of factors: not all flow path angles are possible; the inclination of the path changes as the fluid passes through the screen, eventually being normal to the rear surface; and the screen weave is not axisymmetric about the stagnation point of the jet. The model so far proposed is similar to the previous model, except for the factor ϕ. But it is further postulated that the tangential velocity enters, exits, re-enters, re-exits, etc., the upper layer of wires as the flow is dragged along. Thus, the velocity passing through the screen is only the through-flow V, and not $(V^2 + \phi^2 V_s^2)^{1/2}$. In this model the tangential velocity helps select a flow tube inclination but does not otherwise affect the pressure drop. As in the previous model, the flow tube length is $\ell = bQ(V^2 + \phi^2 V_s^2)^{1/2}/V$. The relation between pressure drop and through-flow velocity for this model is

$$\Delta P = \alpha\left(\frac{a^2 bQ}{2}\right)\mu\sqrt{V^2 + (\phi V_s)^2} + \beta\left(\frac{bQ}{\varepsilon^2 D}\right)\rho V\sqrt{V^2 + (\phi V_s)^2} \qquad (13)$$

or in terms of the constants A and B

$$\Delta P = A\mu\sqrt{V^2 + (\phi V_s)^2} + B\rho V\sqrt{V^2 + (\phi V_s)^2} \qquad (14)$$

This model, like the previous one, has the disadvantage of not modeling large flow angles very well. In fact, it will be seen that equation (13) or (14) only makes mathematical sense over a surface area for which the r-coordinate is less than some R_{max} such that $V^2 \geq (\Delta P/A\mu) - \phi^2 V_s^2$. The reason for this is again neglecting the viscous shear. It ought to be recognized, nonetheless, that this model is valid over a large part of the impingement area. As $V \to 0$ near the periphery, the effect of V_s enters as ϕV_s, and not as the unbounded terms V_s^3/V and V_s^2/V.

Furthermore, for reasonable values of ϕ (less than one), numerical results to be cited later show that the through-flow in the region $r > R_{max}$ ought to be negligible because $\Delta P \approx 0$.

The boundary layer velocity and thickness are estimated from previous results for laminar unidirectional flow along a flat plate (ref. 9). All the tests of reference 4 had laminar boundary layers. Neglecting the radially diverging character of the boundary layer is an approximation, but the correct physical parameters are introduced and the empirical parameter ϕ can also account for the difference between radial and unidirectional flow. The boundary layer thickness is $\delta = 5\sqrt{\mu r/\rho V_r}$ which reduces to $\delta = 6.97\sqrt{\mu R_j/\rho V_j}$ when equation (6) is used for V_r. Since the screen penetrates into the boundary layer by about one-half a wire diameter (b/6 for a twilled Dutch weave) the effective slip velocity V_s can be shown to be

$$V_s = 0.037\left(\frac{r}{R_j}\right)\sqrt{\frac{\rho b^2 V_j}{\mu R_j}} \qquad (15)$$

This expression has been derived by the linearized approximation $V_s = \frac{b}{6}\left(\frac{dV_{BL}}{dz}\right)$ for $z = 0$, where V_{BL} is the laminar boundary layer velocity profile (ref. 9). The numerical constant 0.037 is retained primarily to get the correct order of magnitude for ϕ. (Only the quantity ϕV_s enters the modeling expressions so the pure number 0.037 could in principle be absorbed into ϕ.) Equation (15) has been derived for a twilled Dutch weave, but is valid within a factor of two for other weaves; this extra factor can be absorbed into ϕ.

Equations (14) and (15), together with the impingement pressure expressions, form the proposed mathematical model relating the emergent velocity to the impinging jet characteristics.

Solution for Emergent Velocity

Equation (14) must be averaged over the emerging jet area to predict the average through-flow velocity V_{av} and the flow rate through the screen. The integration needed to obtain this average cannot be done exactly by analytical techniques. Since numerical integration first requires a value of ϕ to be assigned, it is inconvenient to use for verifying the model with experimental data. Instead, an approximate analytical solution is developed in Appendix B. For normal impingement, the integrated result is

$$\frac{V_{av}}{V_j} = \frac{1}{4\pi_1}\left\{\frac{1}{2} + \pi_2 + 2(\phi\pi_3)^2\left[2 + 2(\phi\pi_3)^2 + \pi_2\right] + 4(\phi\pi_3)^2\left[1 + (\phi\pi_3)^2\right]\ln\frac{\phi\pi_3}{\sqrt{1 + (\phi\pi_3)^2}}\right.$$

$$\left. - 2\phi\pi_3\left[2(\phi\pi_3)^2 + \pi_2\right]\sqrt{1 + (\phi\pi_3)^2} + \pi_2^2\ln\left[\frac{\pi_2 + 2\phi\pi_3\left(\sqrt{1 + (\phi\pi_3)^2} - \phi\pi_3\right)}{\pi_2 + 1}\right]\right\} \tag{16}$$

For oblique impingement at 45°, the average through-flow velocity is

$$\frac{V_{av}}{V_j} = \frac{1}{4\pi_1}\left\{0.81 + \frac{5}{2}\pi_2 - 6.79(\phi\pi_2)^3 - 2\pi_2^2\ln\left(\frac{\pi_2 + 1}{\pi_2}\right) - \frac{4}{3}\pi_2^2\ln\left(\frac{4\pi_2 + 3}{4\pi_2}\right)\right.$$

$$+ (\phi\pi_3)^2\left[2 + 2(\phi\pi_3)^2 + \pi_2\right] + 2(\phi\pi_3)^2\left[1 + (\phi\pi_3)^2\right]\ln\frac{\phi\pi_3}{\sqrt{1 + (\phi\pi_3)^2}}$$

$$\left. - (\phi\pi_3)\left[2(\phi\pi_3)^2 + \pi_2\right]\sqrt{1 + (\phi\pi_3)^2} + \frac{\pi_2^2}{2}\ln\left[\frac{\pi_2 + 2\phi\pi_3\left(\sqrt{1 + (\phi\pi_3)^2} - \phi\pi_3\right)}{\pi_2 + 1}\right]\right\} \tag{17}$$

With respect to exact integration, equation (17) is more approximate than equation (16).

The impingement area over which the model for normal impingement yields physically real effects (e.g., $V > 0$ when $\Delta P > 0$), is

$$r \leq R_{max} = 2R_j \left[\sqrt{1 + (\phi\pi_3)^2} - \phi\pi_3\right]$$

A similar but more complicated expression can be derived for oblique impingement.

The degree to which the mathematical model of the throughflow represents reality can be inferred from comparison with test data. A "good" comparison requires that (1) a single value of ϕ correlates all test data for a given screen weave and impingement angle, regardless of fluid properties or jet velocities and diameters, and (2) R_{max} not be too much smaller than $2R_j$. If these requirements are met, then it can be reasonably concluded that the proposed model does incorporate all the important physics of the flow, is valid, and can be used reliabily to predict throughflows.

RESULTS AND DISCUSSION

A substantial amount of test data is available from experiments conducted at NASA-Lewis Research Center. Results for normal impingement have been published (ref. 4), but oblique jet results are available so far only as high-speed 16 mm motion pictures. The tests were conducted in a weightless environment, using a drop tower. Very little liquid penetrated the liquid at low impingement velocities or for very tightly woven screens, and any liquid that did tended either to puddle or to form a small non-growing geyser on the back side. This type of behavior was correlated with a Weber number criterion, which can be used to predict the minimum velocity needed for substantial through-flow. At higher velocities, some of the jet flow penetrated the screen and formed a continually growing geyser. The steady state through-flow measured in these tests constitutes the data used to verify the proposed screen-flow model.

Verification of Model

Twilled Dutch Screens. NASA test results for normal and oblique impingement are shown in Table I. Two other screens (325 x 2300 and 200 x 1400) were also used, but through-flow was not observed with these screens for the tested conditions. Geometrical constants for the screens and physical properties of the fluids are given in Tables II and III. All impinging jets had diameters of 0.625 cm.

For a given screen and set of test conditions, equation (16) for normal or equation (17) for oblique impingement was used to predict the average through-flow velocity as a function of the blockage coefficient ϕ. Typical results for normal impingement are shown in Figure 1. As ϕ increases, the through-flow decreases, which is the desired behavior. The range of ϕ-values needed to correlate the test data is fairly small, regardless of liquid properties or jet velocities, thus tending to validate the assumptions of the model. (The only exception is the TCTFE test using V_j = 125 cm/sec; a value of ϕ = 1.1 is required to predict the through-flow velocity of this test. The correlation proposed in reference 4 also overpredicts this test point, by about 100 percent. It is believed that the data for this test is in error.) There is, at least for this screen, a tendency for the best correlation of ϕ

TABLE I. VALUES OF BLOCKAGE CONSTANT, ϕ, FOR TWILLED DUTCH SCREENS

Screen	Test Liquid	Impingement Velocity, V_j (cm/sec)	Impingement Angle (degrees)	Emergent Velocity, V (cm/sec)	Blockage Constant, ϕ	Predicted Emergent Velocity, cm/sec
200 x 600	Ethanol	269	90	9.9	0.70	8.0
	Ethanol	226	↓	6.2	↓	5.6
	TCTFE*	194	↓	12.9	↓	14.4
	TCTFE	156	↓	7.9	↓	9.5
	TCTFE	125	↓	3.7	↓	6.1
	Ethanol	415	45	23.5	0.35	25.7
	Ethanol	380	↓	22.0	↓	15.8
	Ethanol	345	↓	10.0	↓	6.2
	Ethanol	315	↓	5.6	↓	0.1
	Ethanol	281	↓	4.0	↓	-
	TCTFE	200	↓	19.9	↓	33.6
	TCTFE	185	↓	12.7	↓	26.5
165 x 800	Ethanol	286	90	9.0	0.32	9.2
	TCTFE	170	90	10.8	↓	10.6
	Ethanol	421	45	24.6	0.27	15.5
	Ethanol	411	↓	21.1	↓	15.0
	Ethanol	281	↓	6.3	↓	-
	TCTFE	184	↓	10.9	↓	18.0
	TCTFE	165	↓	6.2	↓	13.5
	TCTFE	141	↓	6.0	↓	8.5
80 x 700	Ethanol	362	90	7.1	0.18	6.6
	Ethanol	330	↓	6.3	↓	5.4
	TCTFE	210	↓	6.4	↓	7.5
	TCTFE	315	45	13.2	0.175	16.9
	TCTFE	275	↓	10.9	↓	10.9
	TCTFE	250	↓	9.9	↓	7.6

*TCTFE = Trichlorotrifluoroethane

TABLE II. SCREEN PARAMETERS

	Twilled Dutch Screens*			Plain** Square Screen
	165 x 800	200 x 600	80 x 700	400 x 400
Viscous resistance coefficient, α	3.3	6.9	5.19	8.61
Inertial resistance coefficient, β	0.17	0.3	0.2	0.52
Screen thickness, b, cm	0.01753	0.015	0.0254	0.00509
Screen-volume void fraction, ε	0.426	0.562	0.369	0.706
Screen pore diameter, D, cm	0.0025	0.00399	0.0025	0.0038
Ratio of surface area to unit volume, a, cm^{-1}	413.6	356	318	514
Tortuosity factor, Q	1.3	1.3	1.3	1.0
Overall screen constants A, cm^{-1}	70889	53990	127276	23229
B	8.54	4.64	19.4	1.40

*Data from ref. 4
**Data from ref. 1

TABLE III. FLUID PROPERTIES AT 20°C

	Liquid	
	Ethanol	TCTFE
Density ρ, gm/cm^3	0.789	1.579
Viscosity μ, gm/cm-sec	0.012	0.007

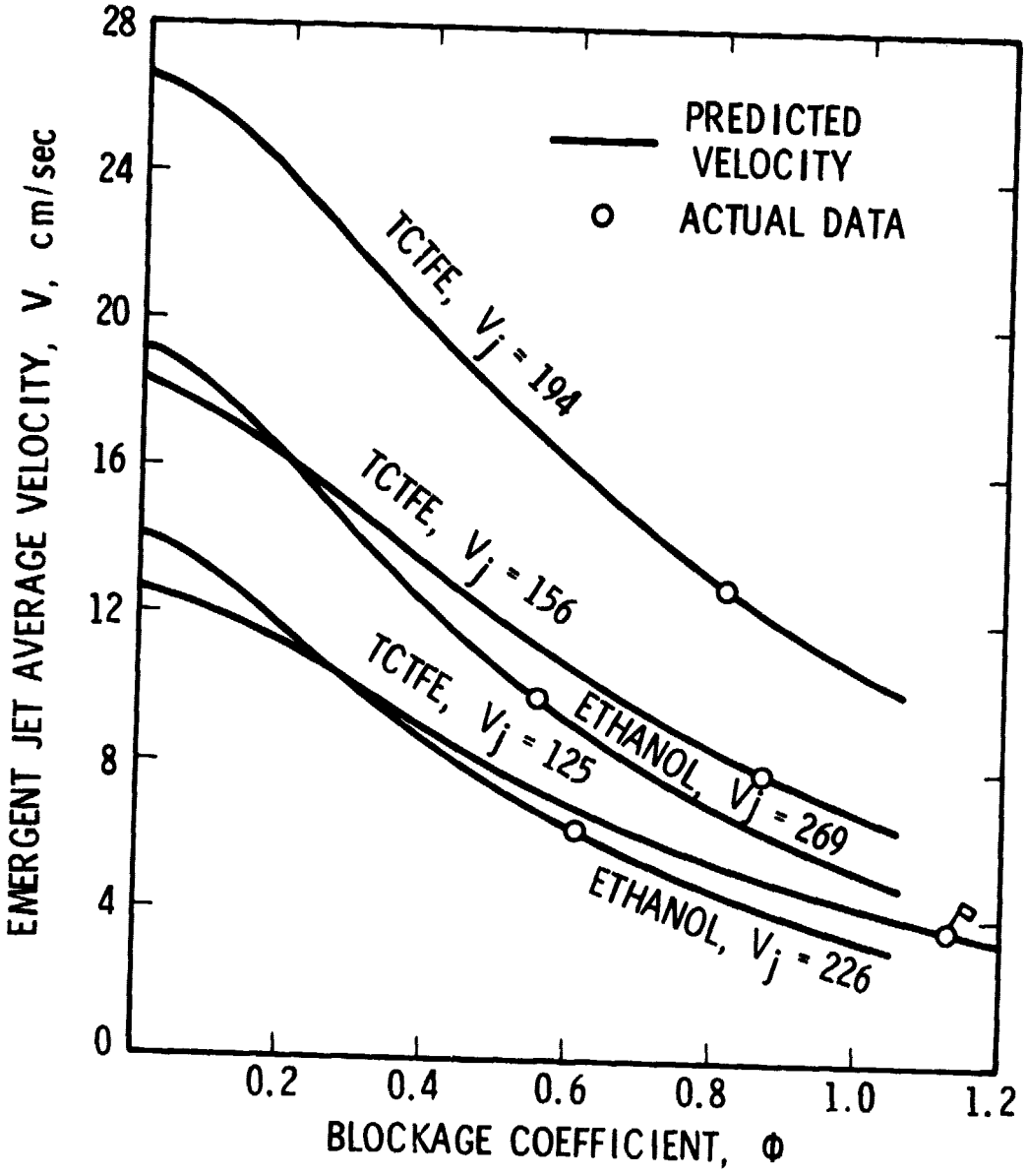

Figure 1. Emergent Jet Average Velocity as Function of Blockage Coefficient. 200 x 600 Screen and Normal Impingement

considering only the TCTFE tests to be slightly greater than the best correlation if only the ethanol tests are considered. One of the premises of the model is that ϕ should not depend on fluid properties, but only on screen and jet geometrical factors. The observed behavior of ϕ is not large enough to invalidate this premise.

Typical results for oblique impingement are shown in Figure 2. There is somewhat more scatter in the value of ϕ needed to predict each test than there is for normal impingement. At least two causes contribute to this. First, the math model itself is less exact because of the approximate pressure distribution used as its basis and the number of mathematical approximations needed to derive equation (17). Second, twilled Dutch screens do not have the same geometrical properties in all lateral directions, but the tests were not all conducted with the same relative orientation of the screen weave and inclined-jet axis. In addition to the scatter, the TCTFE data seem to be correlated by larger values of ϕ than ethanol, similar to the behavior shown in Figure 1. The model fails to predict the test results for ethanol when V_j = 281 cm/sec. In fact even ϕ = 0, which corresponds to a duct-flow model and a jet-impingement pressure distribution, underpredicts the test result slightly. Consequently, this test is neglected in determining the best correlating value of ϕ. An analogous situation (i.e., the best value of ϕ being much smaller for one test of a group) occurred for the 200 x 600 screens with ethanol and V_j = 281 cm/sec. Both of these tests used jet velocities which resulted in little through-flow.

The overall best correlations for ϕ are shown in Table 1. Predicted values of V_{av} using these values of ϕ are also given, except for the two cases mentioned previously for which the model seems to fail. Several conclusions are evident from the tabulated results. Blockage constants for a given screen are always larger for normal impingement than for oblique impingement. Further, the correlation between the measured and predicted emergent-jet velocity is better for normal impingement than for oblique impingement; this is the result of the smaller variation in the best ϕ from one test to another for normal impingement.

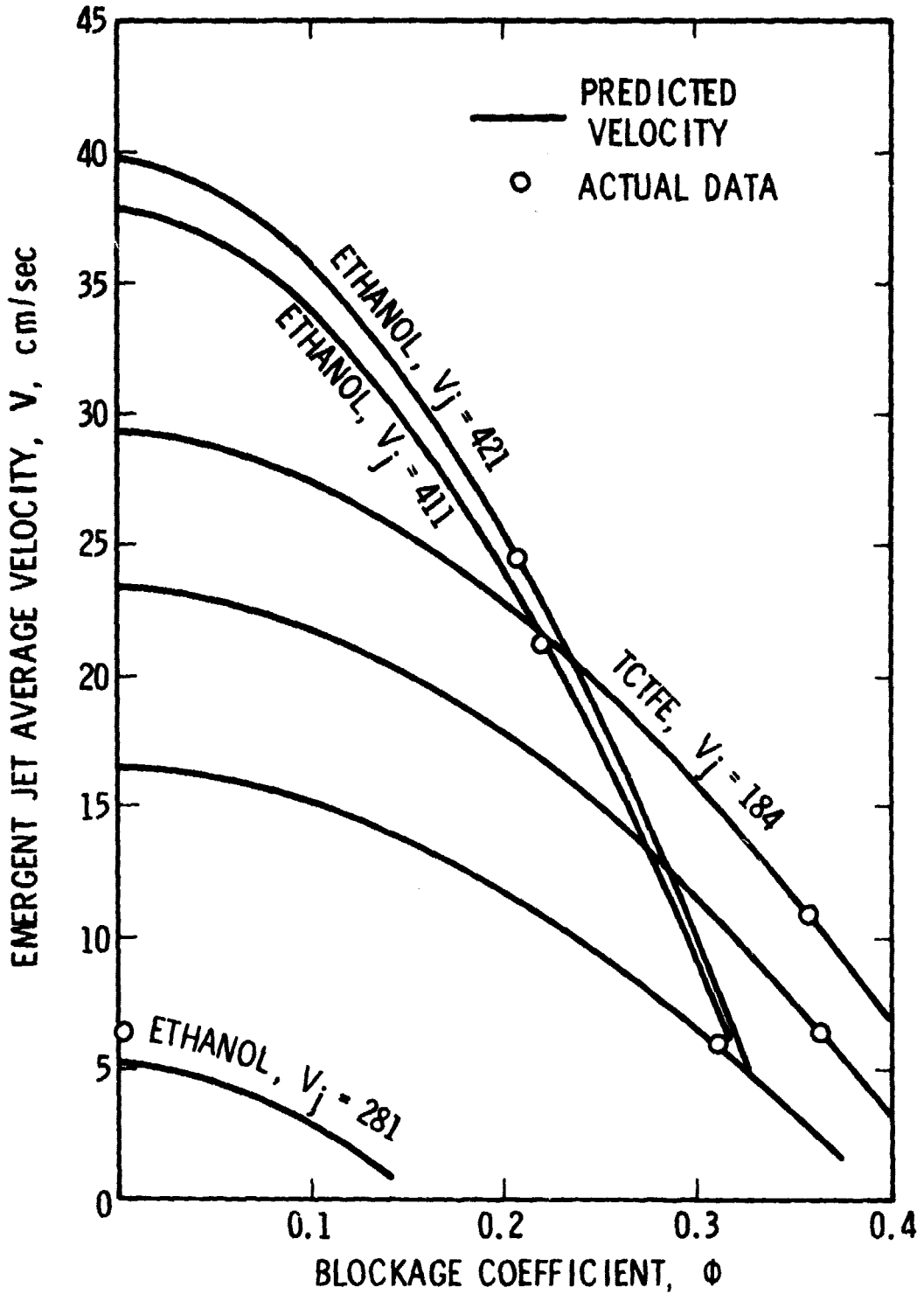

Figure 2. Emergent Jet Average Velocity as Function of Blockage Coefficient. 165 x 800 Screen, 45° Impingement

The largest value of the parameter $\phi\pi_3$, which determines R_{max}, is 0.52, a value that occurs for the 80 x 700 screen and the smallest ethanol jet velocity. From equation (18), $R_{max} = 1.25\ R_j$ for $\phi\pi_3 = 0.52$. For the bulk of the test data, $\phi\pi_3$ is smaller than 0.52 (a value of 0.35 is more appropriate), so the model is mathematically valid over most of the impingement area for most of the tests.

The overall quality of the correlation of the model for normal impingement is shown in Figures 3 and 4, for the 200 x 600 and 80 x 700 screens respectively. Comparisons of predicted and measured velocities are about as good as that shown in reference 1 as the basis for the duct-flow model.

Plain Square Screens. Results from two normal-impingement tests using a 400 x 400 plain square weave screen were also compared to the model. The predicted values for $\phi = 0$ are close to the test results, as might be expected because of the open weave of these screens. Both tests employed ethanol. For V_j = 214 cm/sec, the predicted value from equation (16) with $\phi = 0$ is 28.4 as compared to the test value of 26.5; and for V_j = 246 cm/sec, the prediction is 36.3 as compared to the test value of 30.3. For such relatively open screens, the concept of a blockage coefficient has little meaning, and in fact numerical results show that the predicted through-flow velocity decreases by about only ten percent over a range of ϕ from zero to one.

Note that in making the predictions the general values of $\alpha = 8.61$ and $\beta = 0.52$ (ref. 1) were used since specific data for a 400 x 400 screen is not available. Considering the spread of the data shown in reference 1 about this recommended general correlation, the agreement between test and model predictions for $\phi = 0$ is very good.

Percentage of Liquid Passing Through the Screen

The total flow rate through the screen can be calculated by multiplying the average through-flow velocity by the cross-

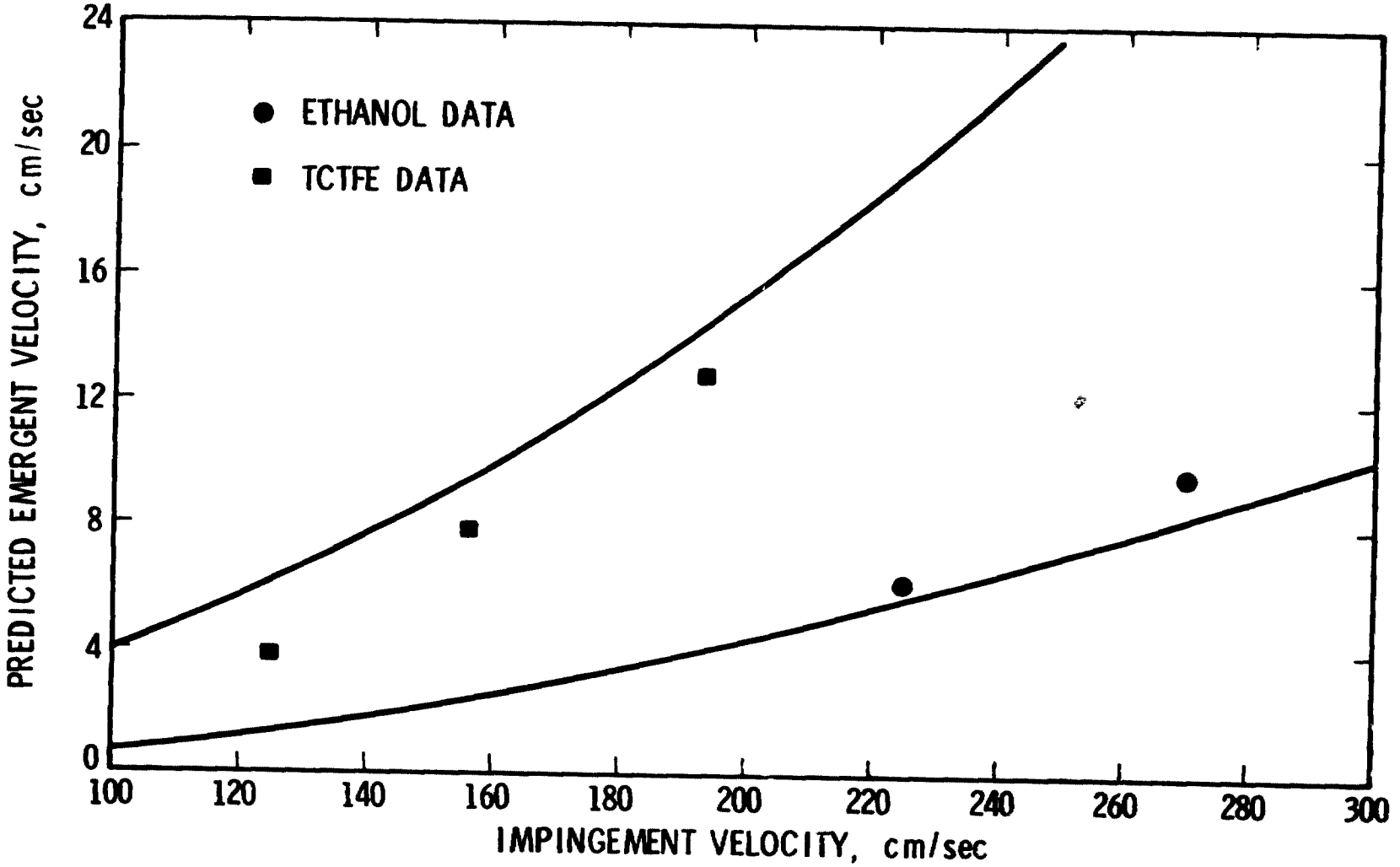

Figure 3. Comparison of Data and Model, Using Best Correlation for Blockage Coefficient, 200 x 600 Screen, Normal Impingement

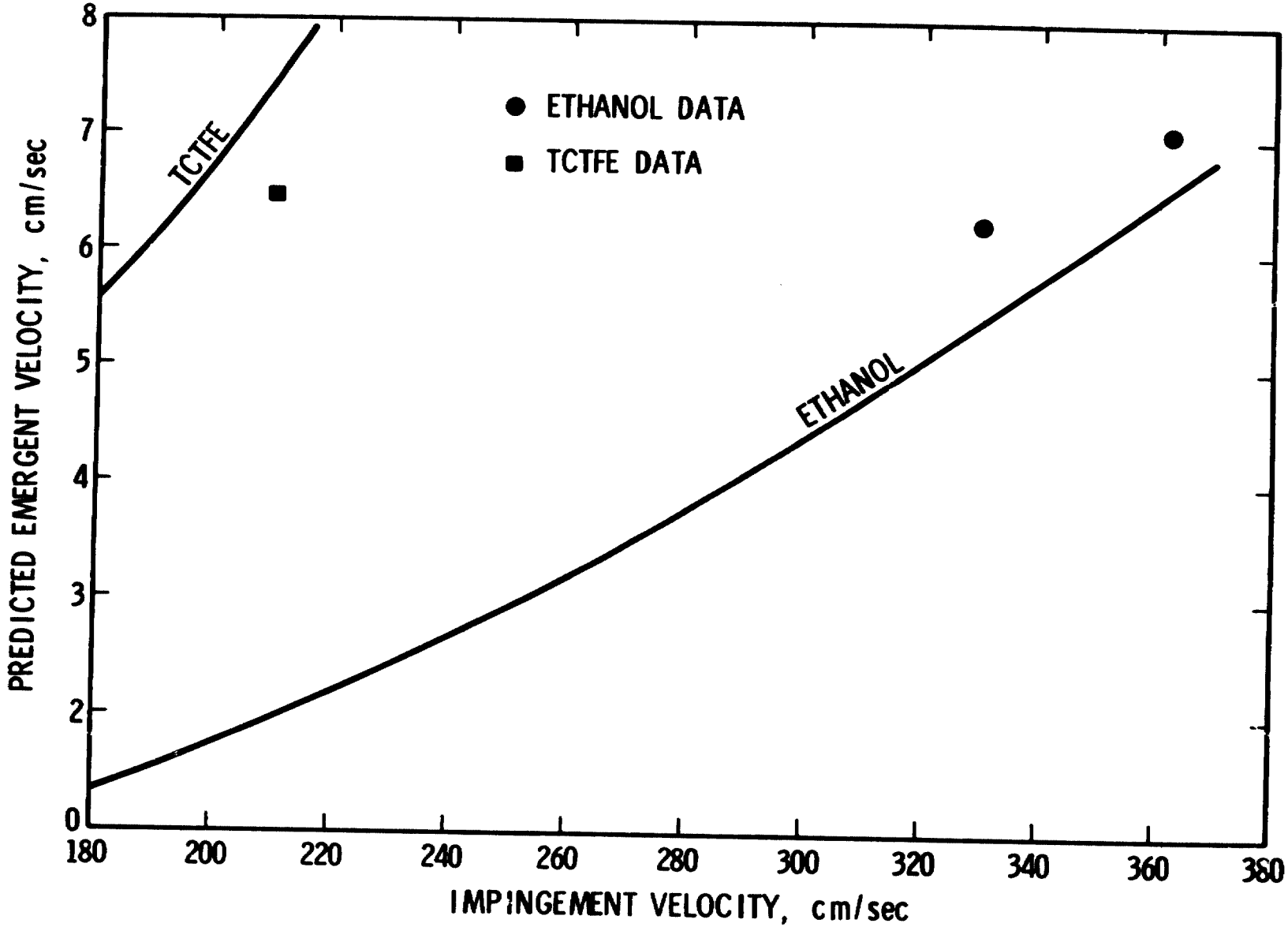

Figure 4. Comparison of Data and Model, Using Best Correlation for Blockage Coefficient, 80 x 700 Screen, Normal Impingement

section area of the emergent jet. For normal impingement, the emergent area is four times the impingement jet area, or 4 πR_j^2. For impingement at 45 degrees, the area can be calculated from the equation of the emergent jet periphery, $r=R_j\ (2 + \cos\theta)$, as explained in Appendix A. This area is 4.5 πR_j^2.

Figure 5, a nondimensional plot of equation (16), can be used to obtain rapid estimates of the average through-flow velocity. This plot also shows that the inertial pressure drop (e.g., the term proportional to ρV^2 in equation (1)) affects the through-flow only for high impingement velocities ($\pi_2 \lesssim 3$). For larger values of π_2 (smaller V_j) the through-flow is a function solely of viscous forces. (The parameter π_2 represents the inertial characteristics, B, of the screen.)

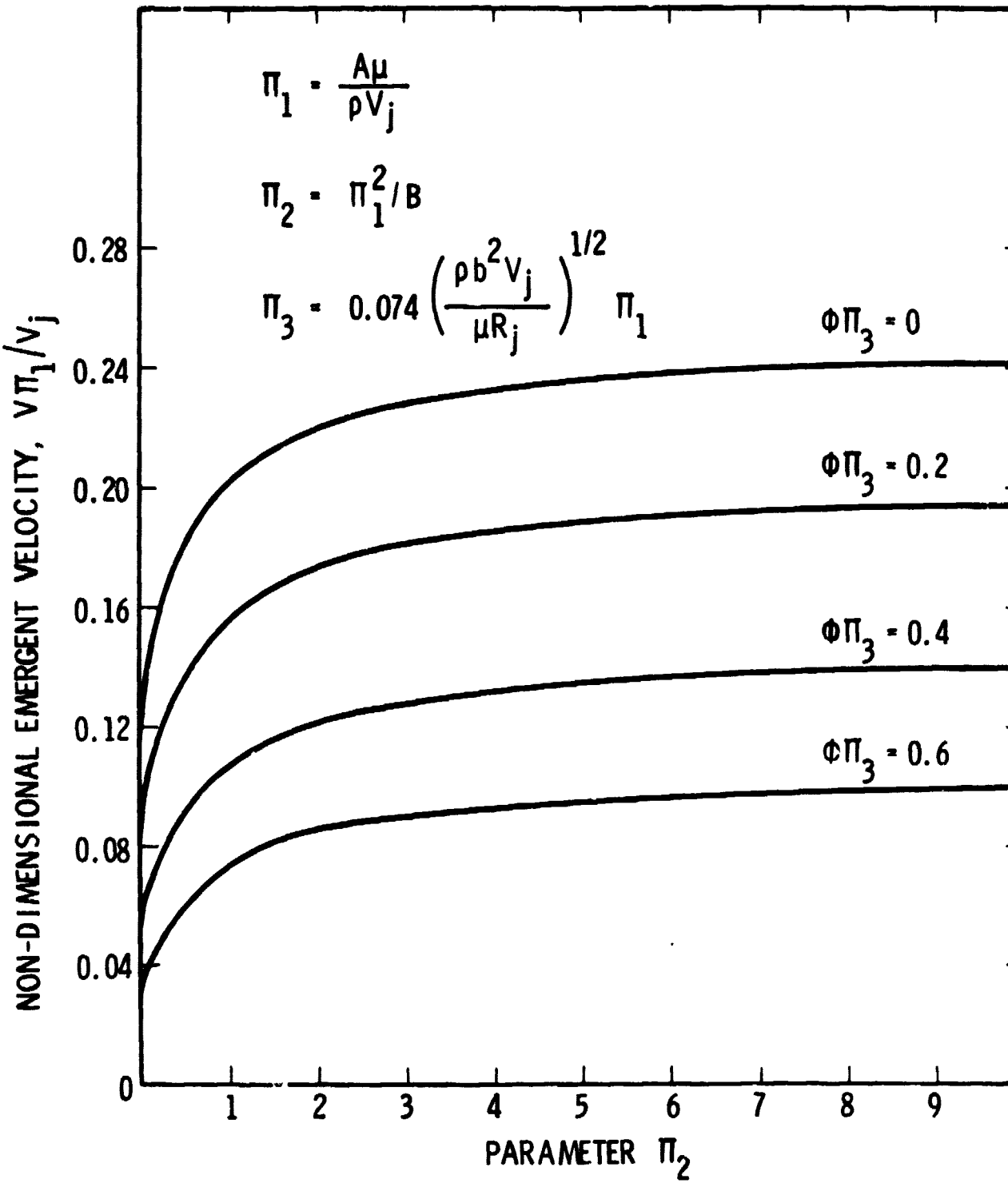

Figure 5. Plot of Equation (16)

CONCLUSIONS AND RECOMMENDATIONS

Physical and mathematical models have been proposed for an unconfined liquid flow impinging upon a fine-mesh screen. The physical basis of the model is the relation between through-flow velocity and pressure drop previously developed for confined duct flow across a screen. This relation has been modified to account for the increase in flow-path length through the screen which results from the deflection of an unconfined flow by the screen. A detailed mathematical development was presented for a circular jet impinging either normally or obliquely (at 45 degrees) on a screen. An important result is that a new parameter, the blockage coefficient, is required to model the impingement flow accurately. Empirical values of the blockage coefficient were determined by comparison with test data from previous studies.

The following conclusions were drawn:

1. The model verifies the previously observed experimental result that the diameter of the emerging jet is about twice as large as the impinging jet.
2. Blockage coefficients depend only on screen geometry and jet impingement angle. Coefficients for normal impingement are somewhat larger than for oblique impingement.
3. The proposed model correlates normal impingement results more accurately than oblique impingement results. This is probably not a basic shortcoming of the model but a result of approximations made in the mathematical development and scatter in the oblique-impingement data.
4. Predicted through-flow velocities for normal impingement, using the recommended correlations for the blockage coefficient, generally agree well (within ±15 percent) with the test data. Predictions for oblique impingement are less accurate.

Additional experiments are recommended to provide an increased degree of confidence in the model.

1. Tests similar to previous NASA studies should be conducted with a wider range of liquids to investigate

possible dependence of the blockage coefficient on liquid properties.

2. Further oblique impingement tests should be conducted, taking care to preserve the same relative orientation of jet and screen-weave geometry from test to test. Other tests should be conducted with the screen weave rotated 90 degrees.

It would also be desirable to run experiments that directly verify the basic premise of the model, namely that the increase of the fluid path length is the cause of the failure of the duct-flow model. Perhaps such tests could be conducted by placing a screen in a duct at an angle to the upstream axis. The duct walls should be removed downstream of the screen, to eliminate wall effects. Measured pressure drop across the screen for a given duct velocity could be compared to tests when the screen is inserted perpendicularly to the axis. Any increase in pressure drop can then be attributed to the increased flow path length of the screen inclined to the upstream flow.

REFERENCES

1. Armour, James C., and Cannon, Joseph N.: Fluid Flow Through Woven Screens. A.I.Ch.E.J., Vol. 14, no. 3, May 1968, pp 415-420.
2. Cady, E. C.: Study of Thermodynamic Vent and Screen Baffle Integration for Orbital Storage and Transfer of Liquid Hydrogen. (MDC-G4798, McDonnell-Douglas Astronautics Co., Contract NAS3-15846) NASA CR-134482, 1973.
3. Blatt, M. H.; Start, J. A.; and Siden, L. E.: Low Gravity Propellant Control Using Capillary Devices in Large Scale Cryogenic Vehicles. Design Handbook. GDC-DDB70-006, General Dynamics/Convair., Contract NAS8-21465, August 1970.
4. Symons, Eugene P.: Normal Impingement of a Circular Liquid Jet Onto a Screen in a Weightless Environment. NASA TM X-3415, August 1976.
5. Bernardi, R. T., Lineham, J. H., and Hamilton, L. H.: Low Reynolds Number Loss Coefficients for Fine-Mesh Screens. Trans. ASME, J. Fluids Engrg., Vol. 98, No. 4, Dec. 1976, pp. 762-763.
6. Schach, W.: Umlenkung eines kreisförmigen Flüssigkeitsstrahles an einer ebenen Platen senkrecht zur Strömungsrichtung. Ingenieur-Archiv, Vol. 6, 1935, pp. 51-59. (Deflection of a Circular Liquid Jet on a Plane Plate Normal to the Stream. Translation Provided by NASA-Lewis Research Center).
7. Schach, W.: Unlenkung eines freien Flüssigkeitsstrahles an einer ebenen Platte. Ingenieur-Archiv, Vol. 5, 1934, pp. 245-265. (Deflection of a Free Fluid Jet at a Flat Panel. NASA TT F-15, 1973).
8. Milne-Thomson, L. M.: Theoretical Hydrodynamics. 4th ed. The MacMillan Co., 1960.
9. Schlichling, H.: Boundary Layer Theory. McGraw-Hill Book Co., 4th ed., 1960.
10. Robertson, J. M.: Hydrodynamics in Theory and Application. Prentice-Hall, Inc., 1965.

APPENDIX A. IMPINGEMENT PRESSURES

Normal Impingement

The only physical parameters needed to describe the ideal flow of a circular jet impinging normally against an impermeable surface are: fluid density ρ, jet velocity far upstream V_j, and jet radius far upstream R_j. Nondimensionalizing the ideal flow equations by these quantities allows all cases to be given by one solution. Velocities are nondimensionalized by V_j, distance by R_j, and pressures by $1/2\ \rho V_j^2$. In terms of a nondimensional stream function ψ, the nondimensional velocities are

$$V_r = -\frac{\partial \psi}{r \partial z} \qquad V_z = \frac{\partial \psi}{r \partial r} \tag{A-1}$$

Conversion of mass is automatically satisfied by ψ, but the condition of irrotationality requires

$$\frac{\partial^2 \psi}{\partial r^2} - \frac{\partial \psi}{r \partial r} + \frac{\partial^2 \psi}{\partial z^2} = 0 \tag{A-2}$$

The boundary conditions that solutions of equation (A-2) must be subjected to are

$$\frac{\partial \psi}{r \partial r} = -1 \qquad r \leq 1,\ z \to +\infty \tag{A-3}$$

$$\frac{\partial \psi}{r \partial r} = 0 \qquad z = 0,\ r \geq 0 \tag{A-4}$$

$$\frac{\partial \psi}{r \partial z} = 0 \qquad r = 0,\ z \geq 0 \tag{A-5}$$

$$\left.\begin{aligned} \psi &= 0 \qquad \text{on jet } \mathcal{C}_L \text{ and } z = 0 \\ \psi &= -1/2 \qquad \text{on free boundary} \end{aligned}\right\} \tag{A-6}$$

Equations (A-6) are a consequence of: (1) the total flow enclosed by the free boundary is $\pi R_j^2 V_j$; and (2) the flow, in terms of the stream function, is -2π times the difference between the values of ψ at the rigid boundaries (or jet centerline) and the free boundary (ref. 10). The negative sign in equations (A-3) and (A-6) implies that the jet approaches with a velocity directed downward.

In setting up the numerical solution, a first guess of the free boundary shape was made and a solution for ψ computed. The equations were written in finite difference form, using a non-uniform grid of 195 points concentrated near the free boundary to improve resolution. A numerical iteration routine was used which does not require matrix inversion, so a desk-top programmable calculator was sufficient. The accuracy of the first guess incorporated the fact that the height of the deflected jet along the wall approaches $R_j^2/2r$ as $r \to \infty$. Several iterations were needed to obtain ±5 percent accuracy for the free-boundary velocity V_j; the corresponding accuracy of the surface pressure integral differed by less than 3.5 percent from $\pi\rho R_j^2 V_j$.

Computed results for the tangential velocity V_r along the surface and surface pressure coefficient $C_p = (p - p_o)/(1/2\ \rho V_j^2)$ are shown in Figure A.1. Also shown is the empirical correlation $C_p = 1 - 0.221(r/R_j)^{2.28}$. This correlation fits the computed curve very well for $r \leq 1.8\ R_j$ and predicts the impact force $\pi\rho R_j^2 V_j^2$ exactly; for $r > 1.8R_j$ the fit is not good, but C_p is so small here that the error caused in through-flow calculations is negligible.

Oblique Impingement at 45°

Numerical solutions for the oblique impingement of a circular jet are beyond the scope of the work, and exact solutions do not exist. Results for a plane jet impacting at 45° (ref. 7) are shown in Figure A-2 (the curve labeled 2 - D, $\gamma = 45°$) along with

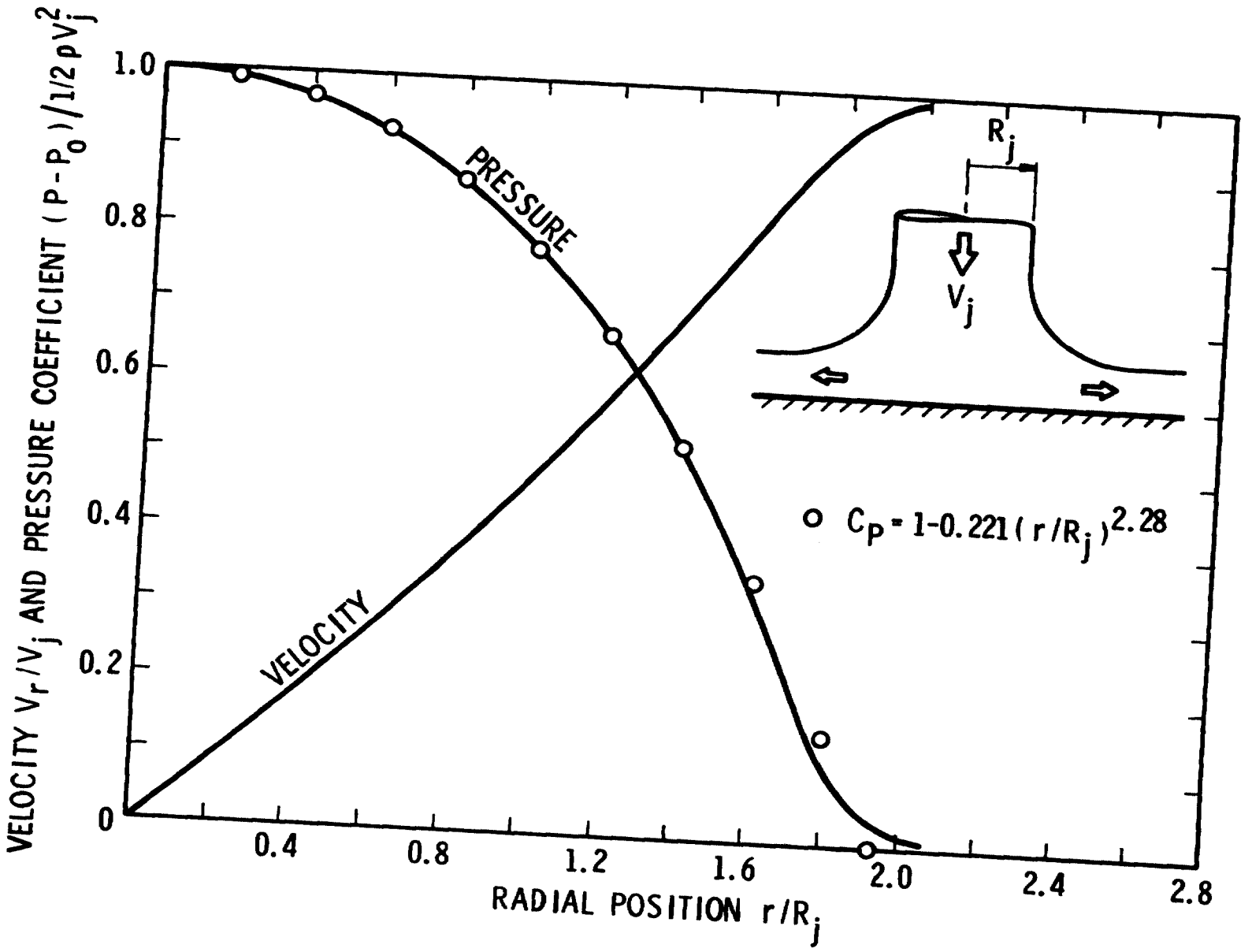

Figure A-1. Pressure and Velocity for Normal Impingement

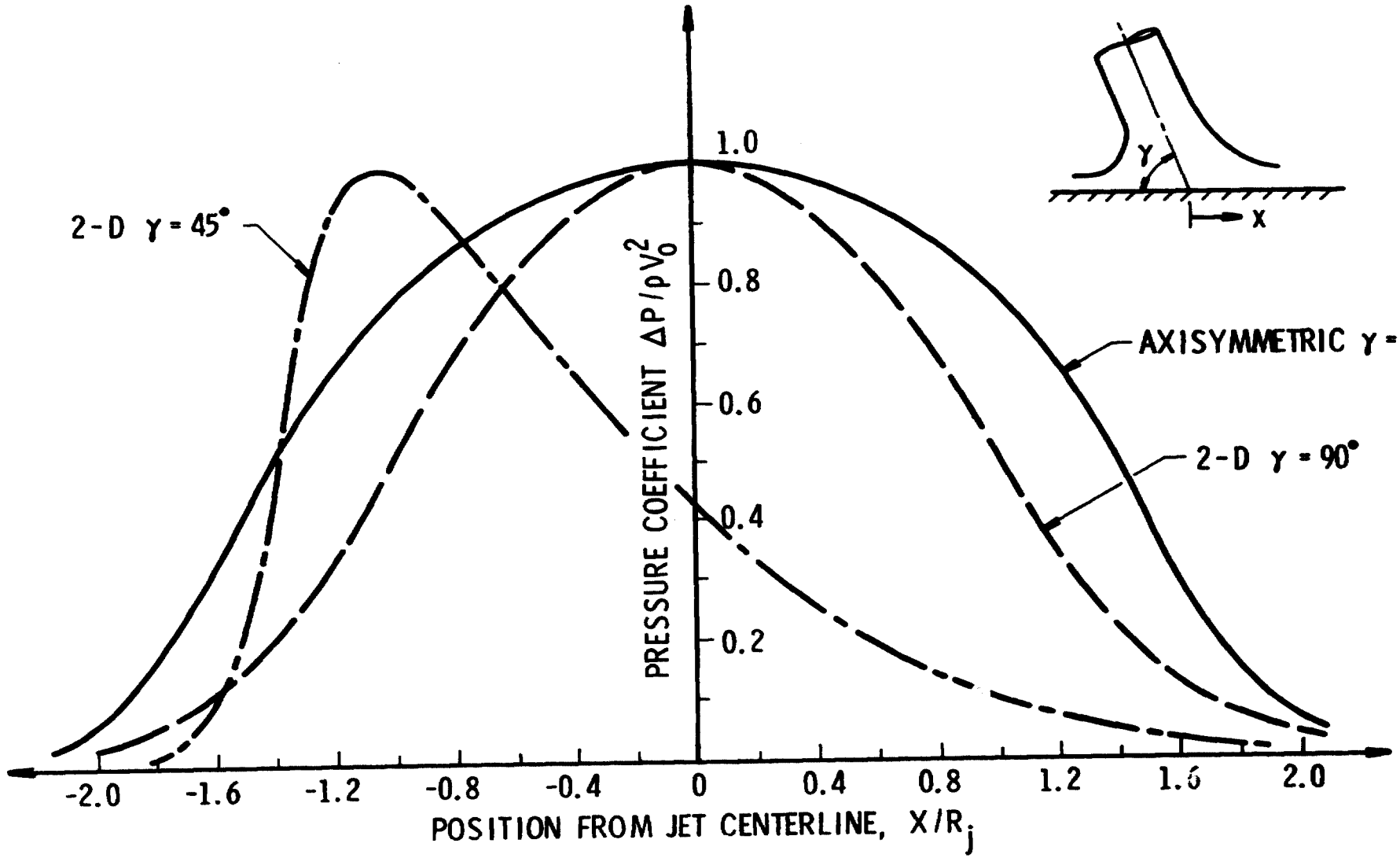

Figure A-2. Impingement Pressures for Various Jets

the axisymmetric case for normal impingement and for a plane jet (ref. 8) impinging normally (the curve labeled 2-D, $\gamma = 90°$). For normal impingement, the axisymmetric pressure distribution is "fuller" than for the plane jet; and for plane oblique jets, the stagnation point moves rearward by about one jet radius. Using these results for guidance, the pressure distribution of a circular jet impinging at 45° is hypothesized to be as shown in Figure A-3. The curves labeled C_{P1}, C_{P2}, and C_{P3} are the pressure coefficients in the coordinate directions shown in the sketch below. The C_{P1}-C_{P2} distribution was obtained from the inclined

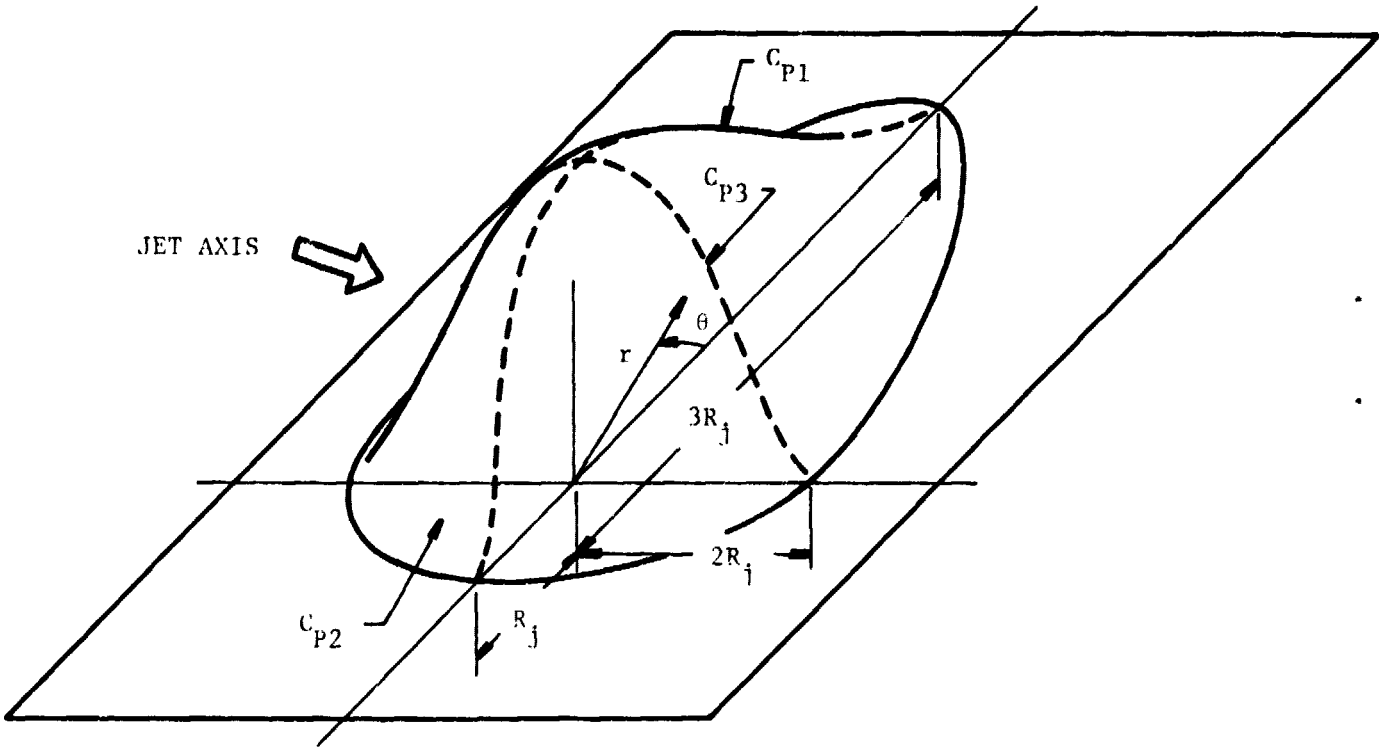

plane jet result shown in Figure A-2, by making it fuller by about the same amount as the difference between the circular and plane jets for normal impingement. The C_{P3} distribution transverse to the jet axis is identical to the pressure for normal impingement of a circular jet. At intermediate locations, the pressure is assumed to vary smoothly between C_{P1} and C_{P3}, or between C_{P2} and C_{P3}; the proposed distribution is

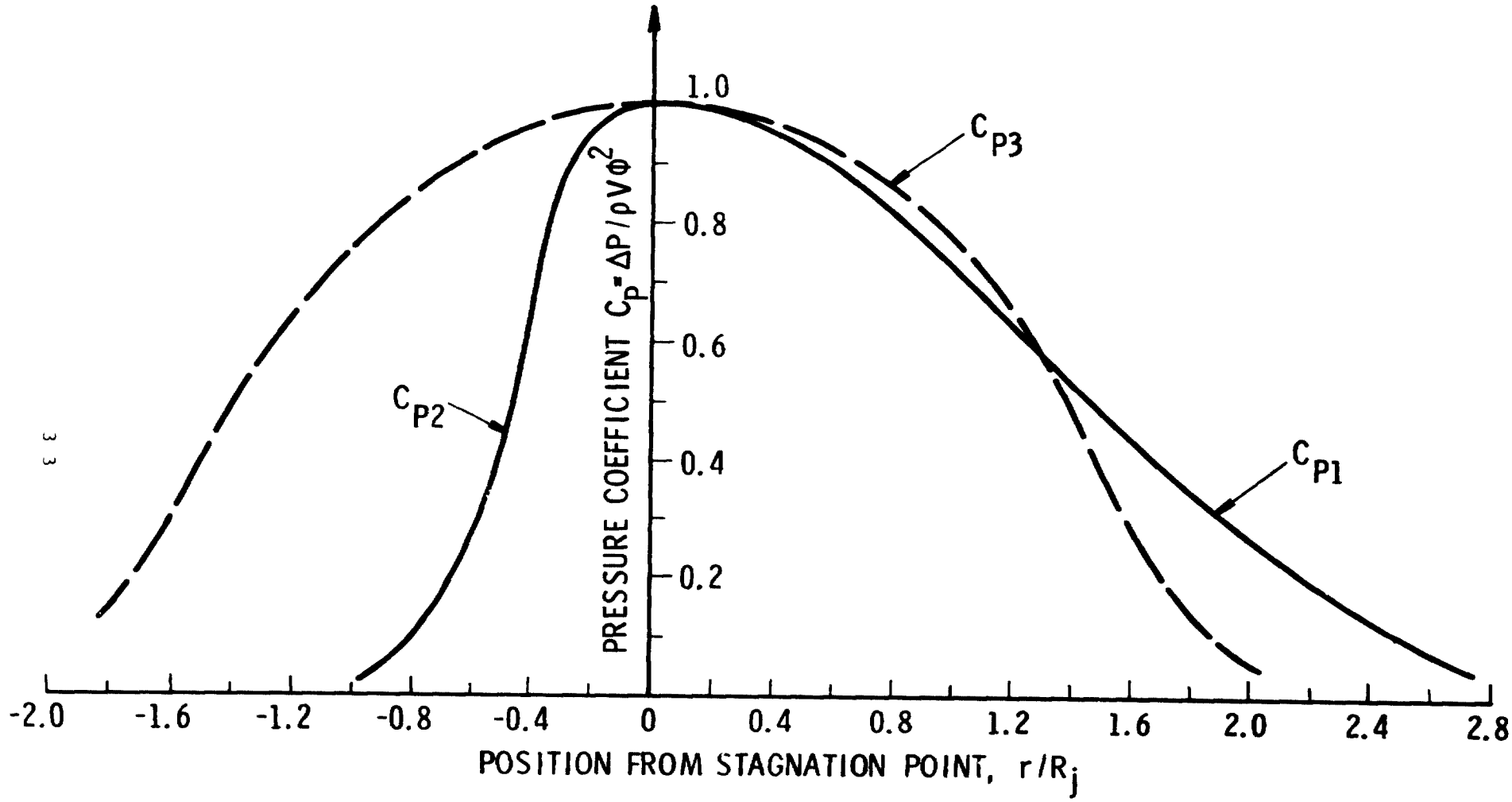

Figure A-3. Pressure Distribution for Circular Jet Impinging at 45°

$$C_p = C_{p1} \cos^2\theta + C_{p3} \sin^2\theta \qquad -90° \leq \theta \leq 90° \qquad \text{(A-7)}$$

$$C_p = C_{p2} \cos^2\theta + C_{p3} \sin^2\theta \qquad 90° \leq \theta \leq 270° \qquad \text{(A-8)}$$

Equations (A-7), with the C_p's taken from Figure A-3, predict an impact force of $0.69\ \pi\rho V_j^2 R_j$, which is very close to the correct impact force $0.707\ \pi\rho V_j^2 R_j^2$.

The region $\Delta P > 0$ extends to $r \approx 3R_j$ in front of the stagnation point, to $r \approx R_j$ behind the stagnation point, and to $r \approx 2R_j$ on either side. A reasonable assumption for the emergent jet area is, therefore,

$$r \leq 2R_j \left(1 + \frac{1}{2} \cos\theta\right) \qquad \text{(A-9)}$$

In the through-flow model, the difference between C_{p1} and C_{p3} is neglected, and equation (A-7) is replaced by

$$C_p \approx C_{p3} \qquad -90° \leq \theta \leq 90° \qquad \text{(A-10)}$$

This is done primarily because an expression of the form $1 - E\,(r/R_j)^2$ where E is a constant, cannot be made to fit the C_{p1} curve with any degree of accuracy. However, a quadratic form is needed to perform the analytical integrations described in Appendix B. The neglected pressures, in any case, are not large. The approximate curve-fits for C_{p2} and C_{p3} discussed in the text overpredict the total force by fifteen percent, as mentioned earlier. This error incurred by neglecting C_{p1} is masked by this approximation.

APPENDIX B. DERIVATION OF THROUGH-FLOW VELOCITY EXPRESSIONS

Normal Impingement

For normal impingement, the model developed in the section titled Modeling of Screen Flow resulted in an expression relating the through-flow velocity V to the pressure ΔP:

$$A\mu\sqrt{V^2 + (\phi V_s)^2} + B\rho V\sqrt{V^2 + (\phi V_s)^2} = \Delta P = \frac{1}{2}\rho C_p V_j^2 \qquad \text{(B-1)}$$

with

$$C_p = 1 - 0.25(r/R_j)^2 \qquad \text{(B-2)}$$

$$V_s = 0.037V_j(r/R_j)\sqrt{\rho b^2 V_j/\mu R_j} \qquad \text{(B-3)}$$

To determine the average through-flow velocity and the total flow rate, equation (B-1) must be solved for V and the solution integrated over the through-flow area. Unfortunately, equation (B-1) cannot be solved exactly, except by numerical methods which require a defined value for ϕ. Therefore, the method of successive approximations, $V = V_1 + \Delta V + \ldots$, is used, where the first approximation V_1 is the solution when the inertial term (the smaller of the two for fine-mesh screens) is neglected. The result for V_1 is

$$V_1 = \sqrt{V_j^2(\rho C_p V_j/\mu A)^2/4 - (\phi V_s)^2} \qquad \text{(B-4)}$$

Equation (B-4) makes sense only for $r < R_{max}$ such that $C_p V_j^2/A\mu > 2\phi V_s$. From equation (B-2) and (B-3), the limiting r is

$$r \leq R_{max} = 2\left\{\sqrt{1 + (\phi\pi_3)^2} - \phi\pi_3\right\} \qquad \text{(B-5)}$$

The linear correction, ΔV, to the first approximation is derived by substituting $V = V_1 + \Delta V$ into equation (B-1) and neglecting higher powers of ΔV.

$$\frac{\Delta V}{V_1} = - \frac{\frac{1}{4}\left(\frac{\rho C_p V_j}{\mu A}\right)^2 B V_j^2}{\left(\frac{\mu A V_1}{\rho}\right) + B\left[\frac{1}{2}\left(\frac{\rho C_p V_j}{\mu A}\right)^2 \rho V_j^2 - (\phi V_s)^2\right]^{1/2}} \qquad \text{(B-6)}$$

(Note that the denominator of the fraction is always greater than zero for $r \leq R_{max}$).

By comparing $V = V_1 + \Delta V$ to the exact solution for $\phi = 0$, it has been found that the accuracy of the approximate solution is ±5 percent. Therefore, additional corrections are neglected, and the solution of equation (B-1) is assumed to be

$$\frac{V}{V_j} = \frac{V_1 + \Delta V}{V_j} = \left[\frac{1}{4}\left(\frac{\rho C_p V_j}{\mu A}\right)^2 - \left(\frac{\phi V_s}{V_j}\right)^2\right]^{1/2} - \frac{\frac{1}{4}\left(\frac{\rho B V_j}{\mu A}\right)\left(\frac{\rho C_p V_j}{\mu A}\right)^2}{\left\{1 + \left(\frac{\rho B V_j}{\mu A}\right)\left[\frac{\frac{1}{2}\left(\frac{\rho C_p V_j}{\mu A}\right)^2 - \left(\frac{\phi V_s}{V_j}\right)^2}{\frac{1}{4}\left(\frac{\rho C_p V_j}{\mu A}\right)^2 - \left(\frac{\phi V_s}{V_j}\right)^2}\right]^{1/2}\right\}} \qquad \text{(B-7)}$$

The average velocity is

$$V_{av} = \frac{1}{4\pi R_j^2} \int_0^{R_{max}} 2\pi r V \, dr \qquad \text{(B-8)}$$

where the flow-through area $\pi(2R_j)^2$ is used to compute V_{av}. Extending the upper limit of integration to $2R_j$ gains nothing since for $r > R_{max}$ the model breaks down, and it has been argued previously that only a negligible amount of flow passes through the area $r > R_{max}$.

After inserting equation (B-2) for C_p and (B-3) for V_s, the first term on the right of equation (B-7) (i.e., V_1) can be integrated:

$$\left(\frac{V_1}{V_j}\right)_{av} = \frac{1}{4\pi_1}\left\{1 + 2(\phi\pi_3)^2 + 4(\phi\pi_3)^2\left[1 + (\phi\pi_3)^2\right]\ell n \frac{\phi\pi_3}{\sqrt{1 + (\phi\pi_3)^2}}\right\} \quad \text{(B-9)}$$

The second term (i.e., ΔV) cannot be integrated until a further approximation is made. Writing this term in the form

$$\frac{1}{4\pi\pi_1}\left\{\frac{\left(1 - \frac{1}{4}x^2\right)^2}{1 + \frac{1}{\pi_2}\left\{\left[\left(1 - \frac{1}{4}x^2\right)^2 + (\phi\pi_3 x)^2\right]^{1/2} + \frac{(\phi\pi x)^2}{2\left[\left(1 - \frac{1}{4}x^2\right) + (\phi\pi x)^2\right]^{1/2}}\right.}\right.$$

where $x = r/R_j$, it can be compared with the simpler expression

$$\frac{1}{4\pi\pi_1}\left\{\frac{\left(1 - \frac{1}{4}x^2\right)^2}{1 + \frac{1}{\pi_2}\left(1 - \frac{1}{4}x^2\right)^2}\right\}$$

The numerators of these two expressions are equal. Comparisons of the denominators are shown in Figure B-1 for various values of $\phi\pi_3 = \gamma$. The simpler expression is an excellent approximation except near $= R_{max}$ (where the curves break upward sharply). It has the additional virture of being integrable. For these reasons, equation (B-6) is replaced by the simpler [illegible]ntegrable expression. The integral can be evaluated by algebraic division

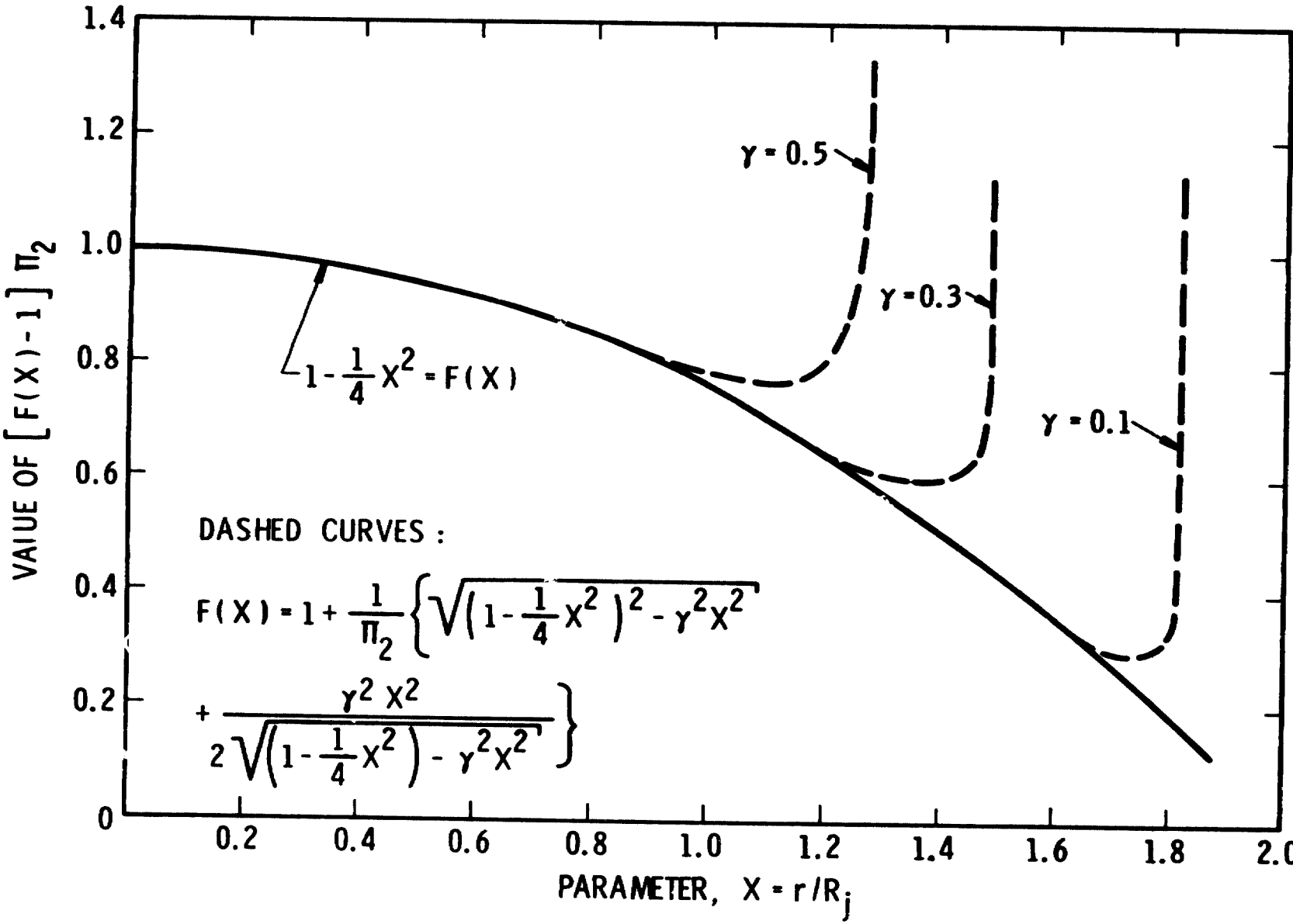

Figure B-1. Plot of Denominator of ΔV and Simple Approximation

$$\left(\frac{\Delta V}{V_j}\right)_{av} = -\frac{1}{4\pi\pi_1}\left(\frac{1}{4\pi R_j^2}\right) *$$

$$\int_0^{R_{max}/R_j} (2\pi R_j^2)\left\{-\pi_2 x^3 + 4\pi_2(1-\pi_2)x + \frac{16\pi_2^2 x}{4(1+\pi_2)-\pi_2 x^2}\right\} dx$$

(B-10)

or

$$\left(\frac{\Delta V}{V_j}\right)_{av} = -\frac{1}{8\pi_1}\left\{1 - 4(\phi\pi_3)^2\left[2 + 2(\phi\pi_3)^2 + \pi_2\right]\right.$$

$$\left. + 4\phi\pi_3\left[2(\phi\pi_3)^2 + \pi_2\right]\sqrt{1+(\phi\pi_3)^2} - 2\pi_2^2 \ln\left[\frac{\pi_2 + 2\phi\pi_3\left(\sqrt{1+(\phi\pi_3)^2} - \phi\pi_3\right)}{\pi_2 + 1}\right]\right\}$$

(B-11)

The total average through-flow velocity is, therefore,

$$\frac{V_{av}}{V_j} = \frac{1}{4\pi_1}\left\{\frac{1}{2} + \pi_2 + 2(\phi\pi_3)^2\left[2 + 2(\phi\pi_3)^2 + \pi_2\right] + 4(\phi\pi_3)^2\left[1 + (\phi\pi_3)^2\right]\ln\frac{\phi\pi_3}{\sqrt{1+(\phi\pi_3)^2}}\right.$$

$$\left. - 2\phi\pi_3\left[2(\phi\pi_3)^2 + \pi_2\right]\sqrt{1+(\phi\pi_3)^2} + \pi_2^2 \ln\left[\frac{\pi_2 + 2\phi\pi_3\left(\sqrt{1+(\phi\pi_3)^2} - \phi\pi_3\right)}{\pi_2 + 1}\right]\right\}$$

(B-12)

Oblique Impingement at 45°

The same general procedure is used for the oblique impingement, although the integrations cannot be perfomed so neatly because of the angular dependence of C_p.

Over the area $-90° \leq \theta \leq 90°$, $r > 0$, the surface pressure for oblique impingement is assumed to be the same as for normal impingement in the approximation used here. Thus, the contribu-

tion to V_{av} of the flow in this region is merely one-half of equation (B-12).

Over the area $90° \leq \theta \leq 270°$ (the area behind the stagnation point) the pressure coefficient C_{p_2} is defined only for $r \leq R_j$, and C_{p_3} defined only for $r \leq 2R_j[1 + (1/2 \cos \theta)]$; see equation (A-10). Because of this, the various integrals must be handled separately. For example,

$$\int_{\pi/2}^{3\pi/2} \int_{0}^{R_{max}} V_1 r \, dr \, d\theta = \int_{\pi/2}^{3\pi/2} \int_{0}^{R_j} V_1 r \, dr \, d\theta + \int_{\pi/2}^{3\pi/2} \int_{R_j}^{2R_j[1 + (1/2 \cos \theta)]} V_1 r \, dr \, d\theta \qquad \text{(B-13)}$$

In the first integral $C_p = C_{p_2} \cos^2\theta + C_{p_3} \sin^2\theta = 1 - x^2(1 - 3/4 \sin^2\theta) = 1 - \xi x^2$, where $\xi = 1 - 3/4 \sin^2\theta$. This is of the same form as the expression used for C_p for normal impingement. Thus, after one integration the first integral is

$$\frac{R_j^2}{2\pi_1} \int_{\pi/2}^{3\pi/2} \frac{1}{\xi} \left\{ -\frac{(\phi\tilde{\pi}_3)^2}{4\xi} \sqrt{(1-\xi)^2 - (\phi\tilde{\pi}_3)^2} + \frac{\xi^2 + (\phi\tilde{\pi}_3)^2}{2\xi} + \frac{1}{2\xi} (\phi\tilde{\pi}_3)^2 \left[1 + \frac{2(\phi\tilde{\pi}_3)^2}{\xi}\right] \ell n \left[\frac{(\phi\tilde{\pi}_3)^2}{(\phi\tilde{\pi}_3)^3 - 2\xi(\xi - 1) - 2\xi \sqrt{(1-\xi)^2 - (\phi\tilde{\pi}_3)^2}} \right] \right\} d\theta \qquad \text{(B-14)}$$

In this expression, $\tilde{\pi}_3 = \pi_3[(1 + 1/2 \cos \theta)^{-3/2}]$; the angular dependence is a result of the tangential velocity relation $V_r = 0.037 \, (r/R_j)[(\rho b^2 V_j)/\mu R_j]^{1/2}(1 + 1/2 \cos \theta)^{-3/2}$, which in turn results from the assumption that the periphery of the emergent jet is given by $r = 2R_j(1 + 1/2 \cos \theta)$ as discussed in Appendix A. Since $(1 - \xi)^2 = (3/4)^2 * \sin^2\theta$, the integral must be evaluated numerically in two parts. The first part covers the range $(1 - \xi) >> \phi\tilde{\pi}$ (say, $\sin^2\theta > 0.1$); the second covers the range

$\sin^2\theta \leq 0.1$, for which $(1 - \xi)^2 - \phi^2\tilde{\pi}_3$ is close to zero. In the first range, the term $[(1 - \beta)^2 - \phi^2\tilde{\pi}_3^2]^{1/2}$ can be expanded in powers of $(\phi\tilde{\pi}_3)^2$ to give $(1 - \xi)\left[1 - \frac{1}{2}\left(\frac{\phi\tilde{\pi}_3}{1 - \xi}\right)^2 - \frac{1}{8}\left(\frac{\phi\tilde{\pi}_3}{1 - \xi}\right)^4 - \ldots\right]$. Powers of $\phi\tilde{\pi}_3$ greater than the second are discarded. With these assumptions, expression (B-14) for $\sin^2\theta > 0.1$ reduces to

$$\frac{R_j^2}{2\pi_1}\int_{\sin^{-1}\sqrt{0.1}}^{\pi/2}\left\{\frac{1}{2} - (\phi\pi_3)^2\left[\frac{\ell n\left(1 - \frac{3}{4}\sin^2\theta\right)}{2\left(1 - \frac{3}{4}\sin^2\theta\right)^2} - \frac{1}{4}\left(1 - \frac{3}{4}\sin^2\theta\right)^{-1}\right]\left(1 - \frac{1}{2}\cos\theta\right)^{-3}\right\}d\theta \qquad \text{(B-15)}$$

This expression can be evaluated numerically since ϕ enters only as a multiplicative constant.

For $\sin^2\theta \leq 0.1$, the remaining part of the first integral is

$$\frac{R_j^2}{2\pi_1}\int_0^{\sin^{-1}\sqrt{0.1}}\left\{\frac{1}{2} + \frac{1}{4}(\phi\pi_3)^2\left(1 - \frac{1}{2}\cos\theta\right)^3\left(1 - \frac{3}{4}\sin^2\theta\right)^{-2}\right\}d\theta \qquad \text{(B-16)}$$

For convenience the limits of integration in both expressions (B-15) and (B-16) have been taken in the quadrant 0 to $\pi/2$, and the term $1 + \cos\theta/2$ has been replaced by $1 - \cos\theta/2$ to account for the fact that $\cos\theta$ is always negative in the actual range, $\pi/2$ to $3\pi/2$.

The average through-flow velocity contribution of the first integral of equation (B-13) is obtained by dividing the integral by $\pi R_j^2/2$. Thus,

$$\frac{2}{\pi R_j^2}\int_{\pi/2}^{3\pi/2}\int_0^{R_j} V_1 r\, dr\, d\theta = \frac{V_j}{\pi_1}\left[\frac{1}{4} - 0.123(\phi\pi_3)^2\right] \qquad \text{(B-17)}$$

The second integral of equation (B-13) is treated similarly. For this integral, an additional restriction must be included. Within these integration limits, $C_p = C_{p3} \sin^2\theta \approx (1 - 1/4\, x^2) \sin^2\theta$, and $C_p \to 0$ as $x \to 2$, which occurs for angles such that $\cos\theta \to 0$. This restriction is analogous to the one for normal impingement (i.e., $r \leq R_{max} \leq 2R_j$) and is caused by a breakdown in the model near the periphery of the emergent jet. The numerical result is

$$\frac{2}{3\pi}\int_{\pi/2}^{3\pi/2}\int_{R_j}^{2R_j[1+(1/2\cos\theta)]} V_1 r\, dr\, d\theta = \frac{1}{\pi_1}\left[0.172 - 1.576(\phi\pi_3)^2\right] \qquad \text{(B-18)}$$

The average of V_1/V_j is the sum of equations (B-17) and (B-18). Next, the average value of $\Delta V/V_j$ is computed, again by similar numerical integration. The result is

$$\left(\frac{\Delta V}{V_j}\right)_{av} = \frac{1}{\pi_1}\left[-0.281 + \frac{\pi_2}{2} - \frac{\pi_2^2}{2}\,\ell n\left(\frac{\pi_2+1}{\pi_2}\right) - \frac{\pi_2^2}{3}\,\ell n\left(\frac{4\pi_2+3}{4\pi_2}\right)\right] \qquad \text{(B-19)}$$

Altogether, the average value of V/V_j is the sum of equations (B-17), (B-18), (B-19) and one-half of (B-12). Thus,

$$\frac{V_{av}}{V_j} = \frac{1}{4\pi_1}\left\{0.81 + \frac{5}{2}\,\pi_2 - 6.79(\phi\pi_2)^3 - 2\pi_2^2\,\ell n\left(\frac{\pi_2+1}{\pi_2}\right) - \frac{4}{3}\,\pi_2^2\,\ell n\left(\frac{4\pi_2+3}{4\pi_2}\right)\right.$$

$$+ (\phi\pi_3)^2\left[2 + 2(\phi\pi_3)^2 + \pi_2\right] + 2(\phi\pi_3)^2\left[1 + (\phi\pi_3)^2\right]\ell n\,\frac{\phi\pi_3}{\sqrt{1+(\phi\pi_3)^2}}$$

$$\left. - (\phi\pi_3)\left[2(\phi\pi_3)^2 + \pi_2\right]\sqrt{1+(\phi\pi_3)^2} + \frac{\pi_2^2}{2}\,\ell n\left[\frac{\pi_2 + 2\phi\pi_3\left(\sqrt{1+(\phi\pi_3)^2} - \phi\pi_3\right)}{\pi_2+1}\right]\right\} \qquad \text{(B-20)}$$

Because of the many approximations made in the numerical integration, equation (B-20) does not represent the "exact" V_{av}/V_j as closely as equation (B-12) does for normal impingement.

APPENDIX C. POROUS MEDIUM MODEL

A two dimensional flow model is examined for simplicity. The pressure distribution on the surface z = 0 is assumed to be

$$\Delta P = \frac{1}{2}\rho V_j^2\left[1 - \frac{1}{4}\left(\frac{x}{W_j}\right)^2\right] \qquad \text{(C-1)}$$

where W_j is the jet half-width. The coordinate system is shown in the sketch. Equation (C-1) is not an accurate representation

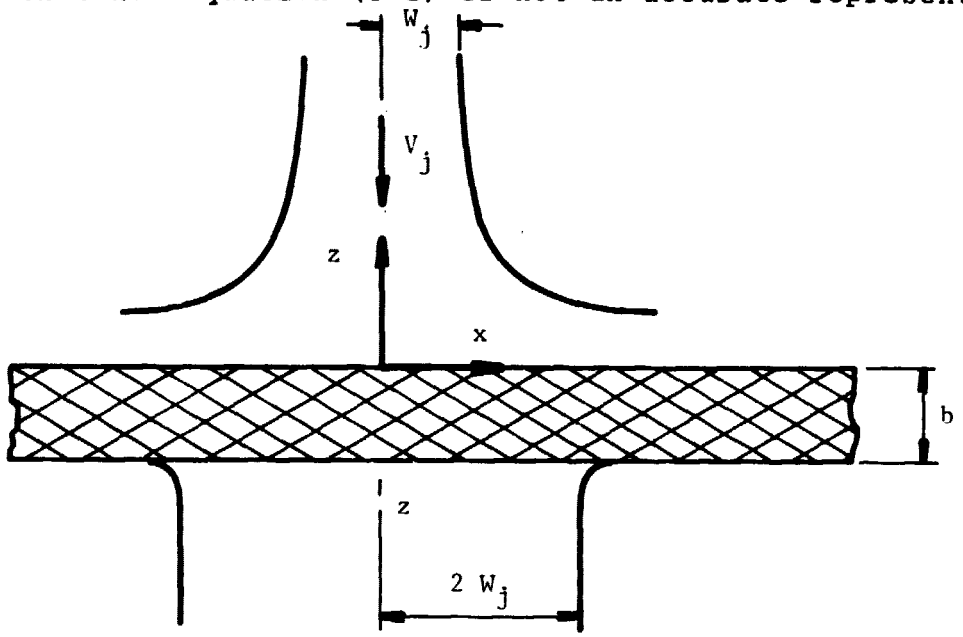

of the impingement pressure for a plane jet but this is of no consequence since only a qualitative model is desired to examine relative effects. The flow law for porous media is

$$V_x = -\frac{K_1}{\mu}\left(\frac{\partial P}{\partial x}\right) \qquad V_z = -\frac{K_2}{\mu}\left(\frac{\partial P}{\partial z}\right) \qquad \text{(C-2)}$$

where K_1 and K_2 can be different to account for different relative resistances across the screen thickness and in the plane of the screen. Conservation of mass, $\partial V_x/\partial x + \partial V_z/\partial z = 0$, gives

$$\frac{\partial^2 P}{\partial x^2} + \left(\frac{K_2}{K_1}\right)\frac{\partial^2 P}{\partial z^2} = 0 \qquad \text{(C-3)}$$

The boundary conditions are

$$P = P_o + \frac{1}{2}\rho V_j^2 \left[1 - \frac{1}{4}\left(\frac{x}{W_j}\right)^2\right] \qquad z = 0,\ x \geq 0 \qquad \text{(C-4)}$$

$$P = P_o \qquad z = -b,\ x \geq 0 \qquad \text{(C-5)}$$

$$\frac{\partial P}{\partial x} = 0 \qquad x = 0,\ -b \leq z \leq 0 \qquad \text{(C-6)}$$

The fourth condition, namely $P \to P_o$ as $x \to \infty$, $-b \leq z \leq 0$, is replaced for convenience by

$$P = P_o \qquad x = 2W_j,\ -b \leq z \leq 0 \qquad \text{(C-7)}$$

This approximation will overestimate the flow within the screen (and underestimate the through flow) since in reality $P > P_o$ at $x = 2W_j$.

The solution of equation (C-3) which satisfied equations (C-5, (C-6), and (C-7) is

$$P = P_o + \sum_{n=1}^{\infty} A_n \cos\left[\frac{(2n-1)\pi x}{4W_j}\right] \sinh\left[\frac{(2n-1)\pi(z-b)}{4W_j(K_2/K_1)^{1/2}}\right] \qquad \text{(C-8)}$$

The constants A_n must be determined from boundary condition equation (C-4), by expanding $[1 - (x/W_j)^2/4]$ into a Fourier series of $\cos[(2n-1)\pi x/4W_j]$ terms. The result is

$$A_n = \frac{1}{2}\rho V_j^2 \left\{ \frac{32(-1)^{n+1}}{\pi^3(2n-1)^3 \sinh\left[\frac{(2n-1)\pi b}{4W_j(K_2/K_1)^{1/2}}\right]} \right\} \qquad \text{(C-9)}$$

A value of $b/2W_j$ corresponding to typical tests of reference 4 is 0.015 cm/0.64 cm = 0.023. Several cases will be examined.

$K_1 = 0$. This corresponds to straight-through flow for which $\partial P/\partial z = (P - P_o)/b$. Thus

$$V_z = - \frac{K_2}{\mu} \left[1 - \frac{1}{4} \left(\frac{x}{W_j} \right)^2 \right] \tag{C-10}$$

and

$$V_{av} = - \frac{1}{4W_j} \int_{-2W_j}^{2W_j} V_z \, dx = \frac{1}{6} \rho V_j^2 \left(\frac{2W_j}{b} \right) \left(\frac{K_2}{\mu W_j} \right)$$

$$= 7.25 \, \rho V_j^2 \left(\frac{K_2}{\mu W_j} \right) \tag{C-11}$$

$K_2/K_1 = 1$. This corresponds to equal flow resistances in the x and z directions. Numerical results are

$$A_1 = 14.28 \, \rho V_j^2 \qquad A_2 = -0.176 \, \rho V_j^2 \quad \ldots \tag{C-12}$$

$$V_{av} = \frac{1}{2} \rho V_j^2 \left(\frac{K_2}{\mu W_j} \right) \left[\frac{1}{8} (14.28 + 0.176 + \ldots) \right]$$

$$= 7.24 \, \rho V_j^2 \left(\frac{K_2}{\mu W_j} \right) \tag{C-13}$$

There is less than 0.07% difference between this flow and the one for straight-through flow.

$K_2/K_1 = 1000$. The results are

$$A_1 = 0.367 \, \rho V_j^2 \qquad A_2 = -0.0013 \, \rho V_j^2 \quad \ldots \tag{C-14}$$

$$V_{av} = \frac{1}{2} \rho v_j^2 \left(\frac{K_2}{\mu W_j}\right) \left[\frac{\sqrt{1000}}{8} (0.367 + 0.0013 + \ldots)\right]$$

$$= 5.83 \rho v_j^2 \left(\frac{K_2}{\mu W_j}\right) \qquad \text{(C-15)}$$

The through-flow is 80 percent of that for when there is no flow in the plane of the screen.

$K_2/K_1 = 10000$. The results are

$$A_1 = 0.0279 \rho v_j^2 \qquad A_2 = -0.75 \times 10^{-6} \rho v_j^2 \quad \ldots \qquad \text{(C-16)}$$

$$V_{av} = 1.39 \rho v_j^2 \left(\frac{K_2}{\mu W_j}\right) \qquad \text{(C-17)}$$

The through-flow is only 19.2 percent of the flow when no in-plane flow exists. Thus, a reduction in flow by a factor of 2, which is needed to correlate the data of reference 4, requires a value of K_2/K_1 greater than 1000 but less than 10,000.

APPENDIX D. SYMBOLS

a	surface area to unit volume ratio of screen, cm^{-1}
A	screen geometrical constant, $\alpha a^2 bQ/E^2$, cm^{-1}
b	thickness of screen, cm
B	screen geometrical constant, $\beta bQ/E^2 D$
C_p	pressure coefficient
D	screen pore diameter, cm
ΔP	pressure drop across screen, N/cm^2
Q	tortuosity factor
r,θ,z	coordinate system centered at jet stagnation point; r,θ in plane of screen, z positive upward.
R_j	impinging jet radius, cm
V	through-flow velocity, cm/sec
V_{av}	average through-flow velocity, cm/sec
V_j	impinging jet velocity, cm/sec
V_s	boundary layer slip velocity, cm/sec
x	r/R_j
α	viscous resistance coefficient
β	inertial resistance coefficient
ε	screen-volume void fraction
μ	liquid viscosity, g/cm-sec
ϕ	blockage coefficient
π_1	dimensionless parameter, $A\mu/\rho V_j$
π_2	dimensionless parameter, π_1^2/B
π_3	dimensionless parameter, $0.074\ (\rho b^2 V_j/\mu R_j)^{1/2}\pi_1$
ψ	dimensionless stream function